Applied Catalysis B: Environmental 130–131 (2013) 197–217

Contents lists available at SciVerse ScienceDirect

Applied Catalysis B: Environmental

journal homepage: www.elsevier.com/locate/apcatb

Review

Pt nanoparticles supported on SBA-15: Synthesis, characterization and applications in heterogeneous catalysis

Junjiang Zhu*, Tao Wang, Xuelian Xu, Ping Xiao, Jinlin Li

Key Laboratory of Catalysis and Materials Science of the State Ethnic Affairs Commission & Ministry of Education, Hubei Province, South-central University for Nationalities, No. 708 Minyuan Road, Wuhan 430074, PR China

ARTICLE INFO

Article history:
Received 4 September 2012
Received in revised form 26 October 2012
Accepted 1 November 2012
Available online 16 November 2012

Keywords:
Pt nanoparticles
SBA-15
Preparation method
Characterization
Catalytic performance

ABSTRACT

This review gave a brief description on the synthesis, characterizations and applications of Pt/SBA-15 in heterogeneous catalysis. Pt/SBA-15 has attracted a great deal of interest in catalysis in the past decades due to its excellent catalytic performances exhibited in the reactions such as CO oxidation, aerobic alcohol oxidation, toluene hydrogenation. Whereas, the preparation of active and stable Pt/SBA-15 material for catalysis use is still a challenging topic, as the surface of SBA-15 is relatively inert and the surface Pt NPs tend to aggregation at high temperatures, or leaching in liquid medium. Thus, for a defined reaction, the selection of a proper method and an understanding to the features of the method are essential before synthesizing Pt/SBA-15 and using it for reactions. In this review, the synthesis method, physicochemical properties and catalytic performances of Pt/SBA-15 prepared by different methods were overviewed. These introductions are base for new researcher working in this field, but are also necessary for experienced scientists who want to explore new fields.

Contents

1. Introduction

Platinum has attracted much attention in catalysis over the decades because of its excellent performances exhibited in reactions such as complete oxidation [1–6], selective oxidation [7–12], dehydrogenation [13–17], and hydrogenation [18–21], either are carried out in gas phase or liquid phase. As well as other noble metals, bulk Pt shows none or little catalytic activity, and only when the Pt catalyst is prepared in nano-size could it show high activity for reactions. It has been suggested that the catalytic performances of noble metals depend intimately on the particle size, which is a crucial parameter influencing the activity, selectivity and lifetime of the catalyst [22]. Alivisatos [23] suggested that dependence of catalytic performances on the particle size is attributed to

* Corresponding author.
E-mail address: ciaczjj@gmail.com (J. Zhu).

0926-3373/$ – see front matter © 2012 Elsevier B.V. All rights reserved.
http://dx.doi.org/10.1016/j.apcatb.2012.11.005

the quantum confinement phenomena derived from the change in the density and effective band gap of the electronic energy level as well as a high ratio of surface to bulk atoms.

In the preparation of Pt catalysts, the most commonly used strategy is to deposit them on high-surface-area supports, with the aim to improve the Pt dispersion and obtain nano-sized Pt particles. In this aspect, the selection of a suitable support and/or preparation method is especially important, as the textural and physicochemical properties of supports have great influence on the formation of Pt particles and consequently the catalytic performances of Pt catalysts. Various works regarding the effect of support on the catalytic performances of Pt catalysts have been reported in the literatures.

The role of support in the catalytic reaction is complex, and is still not clear up to date. Besides as a support to disperse the metal particles, it may also participate in the reaction as part of the active site. Schubert et al. [24] have classified the supports into "inert" and "active" type based on their ability to oxygen activation. The "inert" one is solely as support to disperse the noble metals, while the "active" one acts not only as support but also as part of active site, participating in the reaction. This classification however is not absolute. For example, the magnesium oxide, which is classified as inert support by Schubert et al. [24] was found to be active for oxygen activation in the work of Yan et al. [25] Nevertheless, it is expecting that a support with high surface area would facilitate the dispersion of metal particles and the preparation of high-efficient catalyst. In this review, the use of mesoporous silica SBA-15 as support of Pt nanoparticles (NPs) was described, focusing on the preparation methods, characteristic results, as well as their applications in catalysis.

Comparing to the conventional materials that used as catalyst supports such as Al_2O_3 [26–28], TiO_2 [29–31] and MCM-41 [32–34], SBA-15 has short history, which was synthesized and reported in 1998 by Zhao et al. [35,36] However, it receives rapid attention in materials science and catalysis, and has been proved to be a potential support of heterogeneous noble metal catalysts, due to its straightforward synthesis route, ordered structure, narrow and controllable pore size, high surface area, etc. For example, the wall thickness of SBA-15 is about 3.1–6.4 nm, which gives the material a higher hydrothermal and mechanical stability than, for instance, MCM-41 [37,38]. The hexagonal arrangement of SBA-15 does not possess only the uniformly sized main mesopores, but also the channels of the SBA-15 are interconnected via micropores and secondary mesopores [39–41]. Another important feature of SBA-15 in respect to catalysis is that the surface is relatively inert, but can be activated by in situ substituting the Si atoms with, for instance, Al atoms [42], or by grafting new functional groups through post-synthesis method [43].

Deposition of Pt particles on SBA-15 can be conducted by three strategies: (1) the Pt ions in solution were first adsorbed on the SBA-15, and then reduced to metallic Pt by reducing agent such as H_2 or $NaBH_4$; (2) the Pt ions were first reduced to metallic Pt and then deposited on SBA-15; and (3) in situ incorporation of Pt colloids to the framework during the SBA-15 synthesis process. Based on these strategies, various methods for the preparation of Pt/SBA-15 were introduced, including wetness impregnation (WI), deposition–precipitation (DP), graft hybrid (GH), colloids immobilization (CI), nanoparticle encapsulation (NE). Different methods lead to Pt/SBA-15 exhibiting diverse physicochemical properties, e.g., surface area, pore diameter, and Pt particle size, all of which influence the catalytic performances of the material. Thus, the selection of a proper preparation method is an important step in designing active catalyst for special use.

WI and DP are the most two common methods adopted in the preparation of supported catalysts, as they provide convenient way of depositing Pt particles on SBA-15, the surface of which is inert and is difficult to graft Pt ions in solution directly [44–50]. To activate the SBA-15 so that it can graft the Pt ions in solution, functionalization of the SBA-15 surface by adding additives or surfactants is often conducted, which is the so-called GH method. This method however leads to the NPs formed lacking uniformity in size and shape, and the interaction between the NPs and the support is weak, and therefore agglomeration [50–54] or leaching [36,54–58] of the Pt NPs during the reaction occurs. To control the Pt particle size and obtain uniform Pt NPs, later studies [59–61] proposed to prepare Pt colloids with controllable and uniform particle size before they were deposited on the SBA-15 framework. Depending on whether the Pt colloids were deposited by post-synthesis or by in situ route, it is classified as CI and NE method, respectively. The detailed synthesis route of each method and the corresponding physicochemical characterizations of Pt/SBA-15, together with their catalytic performances in heterogeneous catalysis were demonstrated below.

2. Synthesis and properties of SBA-15

The pioneering work on the synthesis of SBA-15 was reported by Zhao et al. [35] in 1998. Because of the excellent and unique properties of SBA-15, studies [40,41,62–65] on the synthesis and characterization of the SBA-15 were blooming thereafter, to give complete understanding on this material and utilize its advantage for special use, including as catalyst supports. In a typical procedure, the synthesis of SBA-15 is conducted in acidic conditions, using amphiphilic triblock copolymer as structure-directing agent and by a hydrothermal method. The synthesis conditions (e.g., pH, block copolymer, and hydrothermal temperature) can be altered in a wide range, leading to various textural properties while keeping the framework unchanged. Fig. 1 shows the small-angle XRD patterns and N_2 adsorption–desorption isotherms of SBA-15 synthesized using P123 ($EO_{20}PO_{70}EO_{20}$) as structure-directing agent and calcined at 500 °C [35]. The strong diffraction peaks and the type-H1 hysteresis loop indicate that the obtained SBA-15 has ordered and mesoporous structure.

The authors [35] also have investigated the effect of synthesis conditions on the textural properties of SBA-15, by changing the reaction temperature, block copolymer type, and by adding organic swelling agent. Results indicated that the textural properties of SBA-15 can be tuned in a wide range while retaining the periodic structure undestroyed, as shown in Table 1. Furthermore, XRD results showed that no significant change in the diffraction peaks of SBA-15 was observed even after the material was treated in boiling water for 24 h, while those for MCM-41 were complete disappeared under otherwise identical conditions [35]. This suggests that SBA-15 is a better catalyst support in relative to MCM-41 and its texture could be tailored as desired.

Of the textural properties of SBA-15, the porosity receives special interest, as the pore size is an important feature of porous material, deciding the dispersion and size distribution of the supported metal particles, as well as the product distribution of the reaction. As demonstrated in Table 1, the pore size of SBA-15 can be varied from 4.6 to 10 nm by changing the block copolymer and/or reaction temperature. The pore size can further be expanded to 30 nm when swelling agent TMB was added, without destroying the periodic structure [35]. The change in the pore size of SBA-15 synthesized under different conditions was evidenced by TEM images presented in Fig. 2, which shows that even the pore size was increased by a degree of 20 nm, the ordered mesorporous structure remains unchanged.

A great deal of efforts on tailoring the porosity and physicochemical properties of SBA-15 has been devoted thereafter. For example, Kruk and Cao [66] showed that the pore size of SBA-15 can be well tailored using hexane as a micelle expander. Celer and

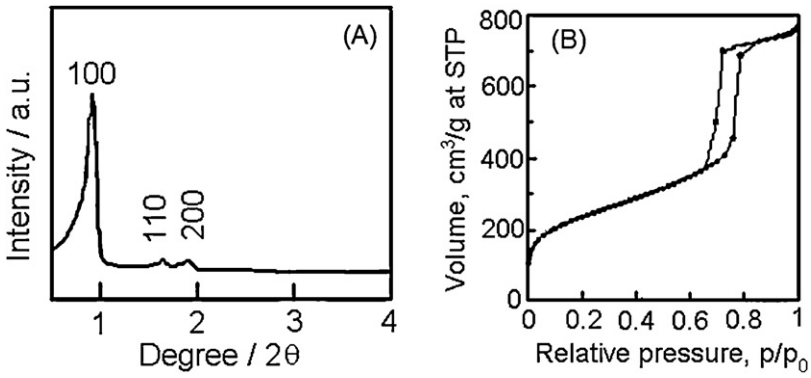

Fig. 1. (A) Powder XRD patterns and (B) N_2 adsorption–desorption of SBA-15 synthesized using P123 as structure-directing agent and calcined at 500 °C for 4 h [35].

Table 1
Effect of synthesis conditions on the physicochemical properties of hexagonal SBA-15 prepared using poly(alkylene oxide) triblock as copolymers. The data were obtained from Ref. [35].

Block copolymer	Reaction temperature (°C)	d(1 0 0) (Å)	BET surface area (m^2/g)	Pore size (Å)	Pore volume (cm^3/g)	Wall thickness (Å)
$EO_5PO_{70}EO_5$	35	118 (117)	630	100	1.04	35
$EO_{20}PO_{70}EO_{20}$	35	104 (95.7)	690	47	0.56	64
$EO_{20}PO_{70}EO_{20}$	35, 80[a]	105 (97.5)	780	60	0.80	53
$EO_{20}PO_{70}EO_{20}$	35, 80[a]	103 (99.5)	820	77	1.03	38
$EO_{20}PO_{70}EO_{20}$	35, 90[a]	108 (105)	920	85	1.23	36
$EO_{20}PO_{70}EO_{20}$	35, 100[a]	105 (104)	850	89	1.17	31
$EO_{17}PO_{55}EO_{17}$	40	97.5 (80.6)	770	46	0.70	47
$EO_{20}PO_{30}EO_{20}$	60	77.6 (77.6)	1000	51	1.26	39
$EO_{26}PO_{39}EO_{26}$	40	92.6 (88.2)	960	60	1.08	42
$EO_{13}PO_{70}EO_{13}$	60	80.6 (80.5)	950	59	1.19	34
$EO_{19}PO_{33}EO_{19}$	60	74.5 (71.1)	1040	48	1.15	34

[a] Reaction at 35 °C for 20 h, then heating to the higher temperature for 24 h, or for the second entry for 80 °C, 48 h.

Jaroniec [67] reported that SBA-15 synthesized under microwave conditions and at high temperatures (e.g., 160, 180, and 200 °C) showed better thermal stability than those synthesized at commonly used temperatures either under conventional or microwave conditions. We [64] recently reported that the porosity of SBA-15 can be tailored by adding poly(vino alcohol), PVA, as copolymer, with other synthesis conditions similar to those reported by Zhao et al. [35]. Results indicated that the surface area of SBA-15 increased significantly after the addition of PVA, while the primary pores kept unchanged no matter the amount of PVA was added, as demonstrated by the N_2 adsorption–desorption isotherms shown in Fig. 3. Further studies indicated that PVA alone also has the ability to create pores in the silica and it will not interfere with the P123 in creating pores. Consequently, we assumed that the increase of surface area is due to the formation of new pores created by the removal of PVA in the SBA-15 framework, as proposed in Scheme 1.

3. Pt/SBA-15 synthesized by wetness impregnation (WI) method

Wetness impregnation is the simplest method and is widely used for the preparation of supported catalyst. In this method, $H_2PtCl_6{\cdot}6H_2O$ aqueous solution with defined concentration and volume was poured to a container loading with SBA-15 material, of which the volume is similar to that of the $H_2PtCl_6{\cdot}6H_2O$ aqueous solution. The resulting sample was then dried and calcined/reduced (in H_2) at certain temperature for some time to obtain the Pt/SBA-15_WI sample (*note*: "Pt/SBA-15_M" means that the Pt/SBA-15 was prepared by "M" method, the same meaning below). The Pt loading can be easily controlled by varying the mass ratio of $H_2PtCl_6{\cdot}6H_2O$ to SBA-15. Detailed synthesis procedures of this method are shown in Scheme 2 (left).

Because the WI method is often conducted at room temperature and no drastic condition is required, changes in the framework and pore structure of SBA-15 after Pt deposition could be neglected, as evidenced by the N_2 adsorption–desorption isotherms, Fig. 4 [68,69]. This offers a convenient way of comparing the catalytic performances between SBA-15 and Pt/SBA-15, to indicate the role of Pt NPs played in the reaction. Whereas, it should be noted that the deposition of Pt NPs would block the pores, and/or be attached on the pore wall of SBA-15, leading to decreased surface area and pore volume, in relative to those of SBA-15.

The retained pore structure of Pt/SBA-15_WI was also confirmed by the small-angle XRD patterns, Fig. 5A, which shows three well-defined peaks assignable to (1 0 0), (1 1 0) and (2 0 0) face of SBA-15. For XRD patterns measured at wide diffraction angles, Fig. 5B, three new diffraction peaks at $2\theta = 39.78°$, 46.28° and 67.48° appeared after Pt deposition, and were assigned to the (1 1 1), (2 0 0) and (2 2 0) face of cubic Pt, respectively, suggesting the existence of Pt. The weak intensity of the diffraction peaks implied that the Pt has small particle size. Indeed, calculation from the Scherrer formula using the most intense reflection of Pt(1 1 1) recorded at 2θ of 39.7° indicated that the Pt crystal size is ca. 5.4 nm.

Other than the framework structure, the surface chemistry of SBA-15 is sensitive to the environment and would be altered after the Pt deposition. The changes in the surface chemistry were differentiated by an infrared spectrum, as demonstrated in Fig. 6(A). For pure SBA-15, three sets of bands with prominent absorptions at around 7300, 5270 and 4520 cm^{-1} appeared [68,69], indicating that it has the characters of siliceous materials [70–74]. In the first set, the peak centered at 7326 cm^{-1} is attributable to the first overtone of the stretching frequency of silanols (ν_{OH}) [70–72], while those at 7141 and 6856 cm^{-1} are due to the isolated water molecules hydrogen bonded to silanol groups [71], and the shoulder at 7425 cm^{-1} is to silanols that are perturbed by the interparticle contact [72,75].

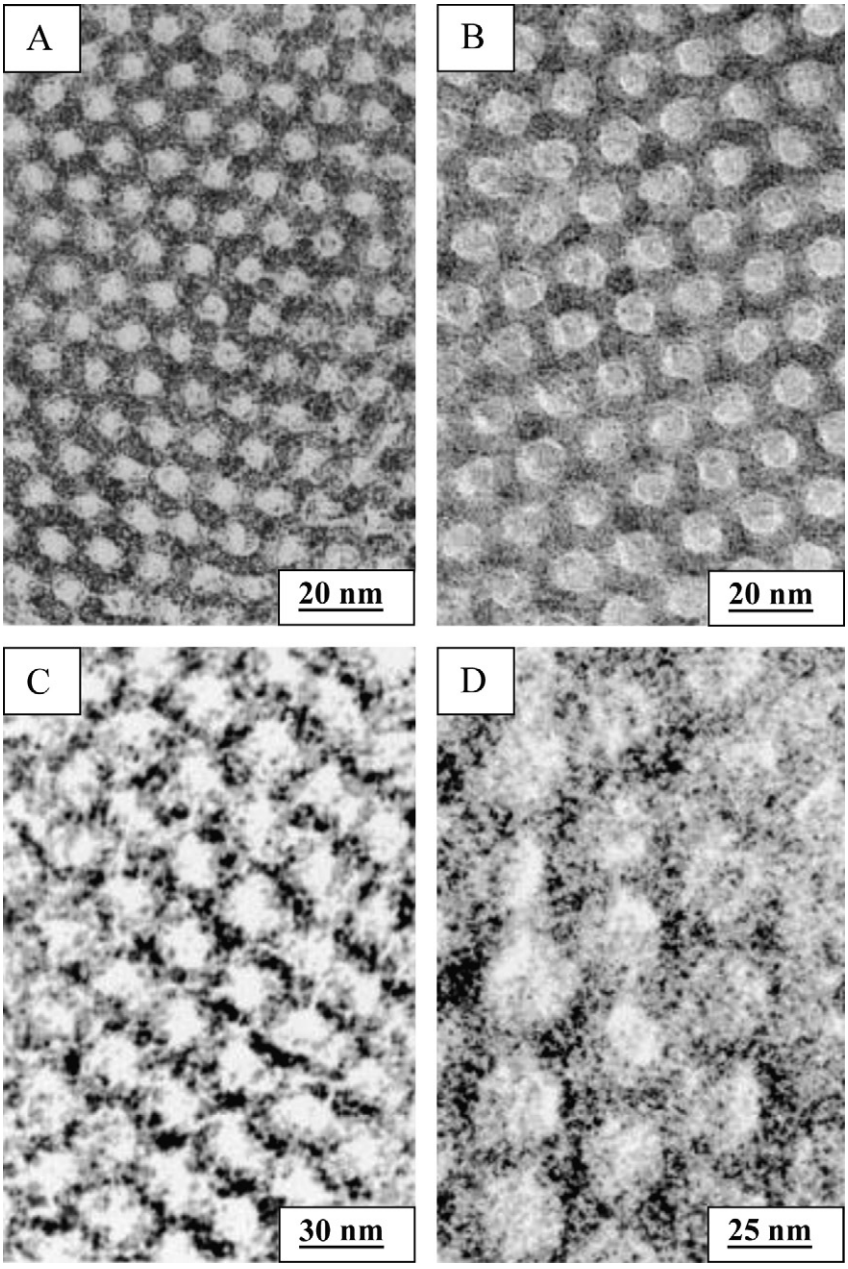

Fig. 2. TEM images of calcined hexagonal SBA-15 mesoporous silica with different average pore sizes, from BET and XRD results (24): (A) 60 Å, (B) 89 Å, (C) 200 Å, and (D) 260 Å [35].

In the second and third sets, each contained one prominent peak that located at around 5270 and 4520 cm^{-1}, respectively. These two peaks are assignable to the combination of stretching and deformation vibrations of water [71], and combination of the fundamental OH^- stretching of the isolated SiOH groups with the fundamental symmetric stretching mode of silica network at 800 cm^{-1} [72], or to the combination of the stretching and deformation vibration of —SiOH groups [75], respectively.

After Pt deposition, three sets of absorption bands locating at 7600–6500, 6000–5000 and 5000–4200 cm^{-1} appeared, Fig. 6(B)–(D). The decrease in the intensity of the first overtone band (Fig. 6(B)) indicated that the silanol number is decreased after Pt deposition, while the increased peak intensity at around 5270 cm^{-1}, Fig. 6(C), revealed that the amount of water in Pt/SBA-15 is higher than that in SBA-15, due to the aqueous environment used in this process. No significant change in the peak intensity and peak shape was observed in Fig. 6(D), suggesting that the Pt addition does not interfere much on the original OH^- and/or SiOH groups. Further studies indicated that the addition of Pt can retard changes occurring in the SBA-15 structure, but causes much loss of silanols [69].

Although no obvious change in the matrix structure of SBA-15 was observed in the N_2 adsorption–desorption isotherms before and after Pt deposition, the loss of silanols (see Fig. 6) suggested that the framework was altered, as supported by the ^{29}Si MAS NMR spectrum shown in Fig. 7, which represents the situation of Si atoms in the SBA-15 matrix structure. In the ^{29}Si MAS NMR spectrum, three Q^n bands could be classified depending on the binding environments. For silica materials, the low intensity Q^2 peak at −91 ppm is assigned to the germinal silanol groups ($(SiO)_2Si(OH)_2$, the Q^3 at −101 ppm is to the isolated silanols ($(SiO)_3Si(OH)$, and the Q^4 band centered at −110 ppm is to silicons of the ($(SiO)_4Si$ type [76,77]. The

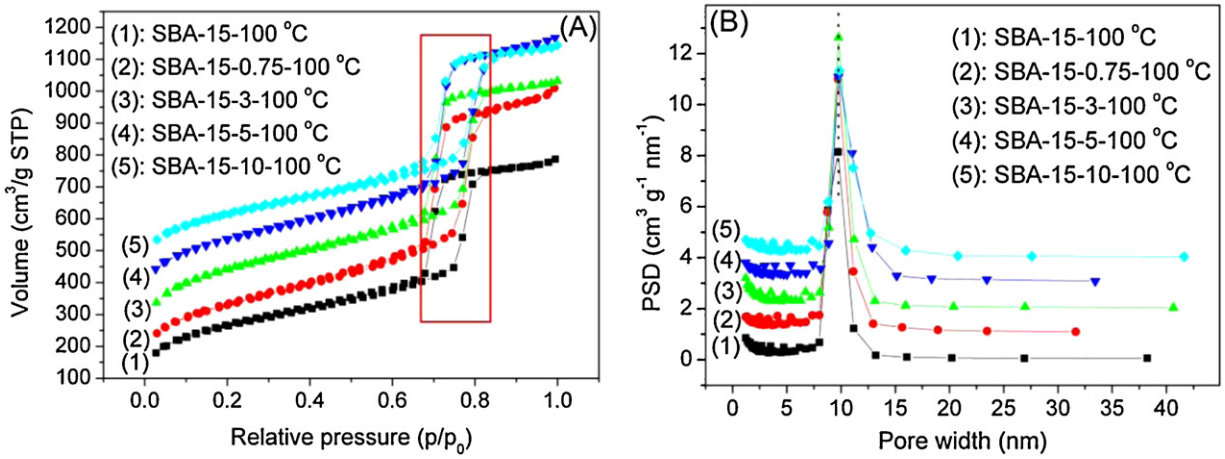

Fig. 3. (A) N_2 adsorption–desorption isotherms for SBA-15 synthesized with different PVA contents and aged at 100 °C, and (B) the corresponding pore size distribution derived from the BET isotherms.

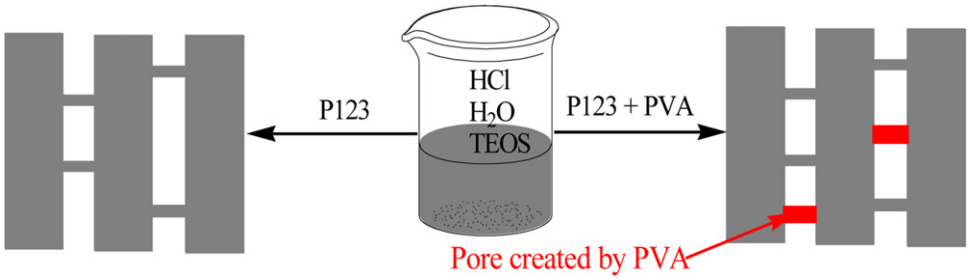

Scheme 1. Role of PVA in the formation process of SBA-15.

Q^4 band represents a silicon population in a fully condensed framework, while the Q^2 and Q^3 bands represent incompletely condensed silicon atoms [69]. In the case of SBA-15, the three Q^n bands were overlapped and only one apparent peak was observed, suggesting a broad range of Si—O—Si (T—O—T) bond angles with a framework lacking precise repeats of Si positions at the second nearest neighbor (T—T) scale [78], similar to that observed for amorphous silicas [79] and mesoporous silica MCM-41 [78]. Compared with that of SBA-15, the Q^n bands of Pt/SBA-15 were better resolved and one shoulder peak appeared, suggesting a short-range order of the silica framework due to the consumption of silanol in the dehydroxylation step caused by the additional calcination [69].

Besides the structure characters of SBA-15, the particle size and size distribution of the Pt NPs are also important parameters in deciding the catalytic performances of the supported Pt catalyst. For this, TEM measurement, which provides microcosmic information on the surface of the materials, would be a powerful means. As illustrated in Fig. 8, the sample Pt/SBA-15_WI remained the ordered structure of SBA-15, and that the Pt NPs were well dispersed on the SBA-15, Fig. 8(A), with particle size in the range of 3–8 nm [80]. The

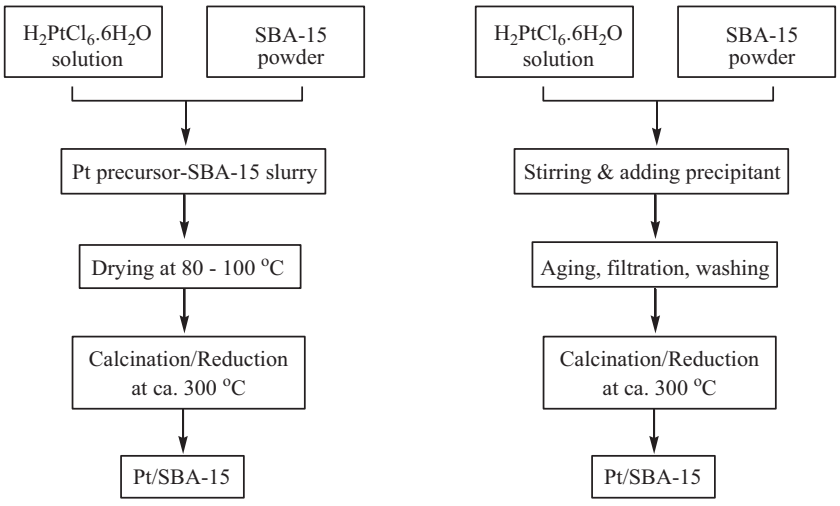

Scheme 2. Assemble line for the preparation of Pt/SBA-15 catalyst by WI and DP method, respectively.

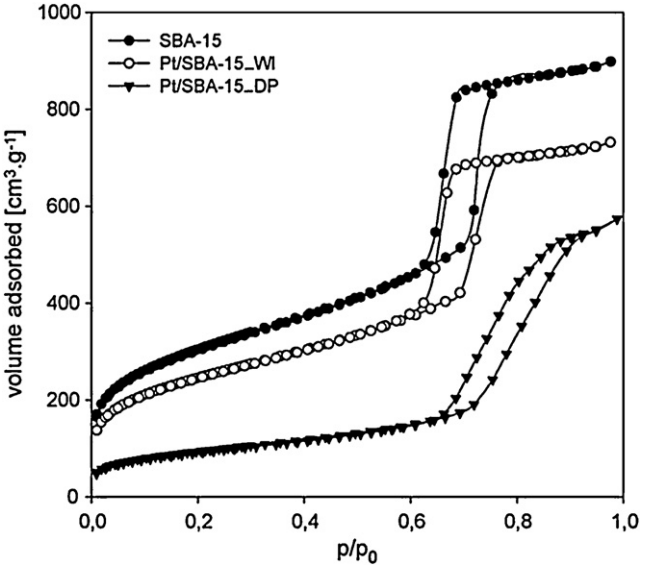

Fig. 4. N_2 adsorption–desorption isotherms of SBA-15 and Pt/SBA materials prepared by WI and DP methods [69].

wide ranging of Pt particle size allows the Pt NPs locating either inside (Fig. 8(B)) or outside (Fig. 8(C)) of the channels of SBA-15. Also, depending on precursors the platinum can be existed in the channels of SBA-15 in nanowires form, Fig. 8(D) [81].

It however should be noted that in this method, mobilization and aggregation of Pt atoms on the SBA-15 surface occurs readily, and big Pt particles would be formed in the final product, leading to low efficiency for catalytic reactions. Furthermore, as this method does not require filtration procedure, residues of chloride ion, which comes from the Pt precursor (e.g., $H_2PtCl_6{\cdot}6H_2O$) and is poisonous to various catalytic reactions, in the catalyst cannot be avoided.

4. Pt/SBA-15 synthesized by deposition–precipitation (DP) method

The principle of DP method is based on the solubility of the aimed cations at certain conditions. As long as a cation is precipitable, the corresponding catalyst can be prepared by DP method. The DP method provides a way of preparing active phase with high loading, high dispersion and small particle size. In this method the deposition of metal NPs proceeds in three stages: supersaturation, nucleation, and growth of the precipitated particles on the support [82,83]. The metastable supersaturated region can be approached either by increasing the concentration through evaporation of a solvent, lowering the temperature of a system, or by increasing the pH value in bulk phase [82,83]. Usually, the precipitation is in hydroxide form, which can be readily decomposed into oxides and water, and no unwanted residue retaining in the catalyst. For Pt/SBA-15, a synthesis procedure reported by Blekkan et al. [68,69,80], is as below: 3 g of SBA-15 was first exposed to an aqueous solution containing urea (deionized water 250 mL, urea 0.026 g) under N_2 atmosphere; the resulting suspension was then acidified by 0.1 M HNO_3 (to pH 3.5) and kept at 90 °C for 20 h; afterwards, the solids were recovered by filtration and washed by deionized water (200 mL); the washed material was dried in an oven at 80 °C for 17 h and finally calcined in flowing air at 300 °C for 2 h.

pH value of the solution is a crucial factor of this method, as it decides the deposition process of the Pt NPs. Blekkan et al. [80] investigated the change of pH value with the reaction time in the preparation of Pt/SBA-15, finding that the pH value increases at the beginning, then reaches a constant, and thereafter a slight decrease with the reaction time, as shown in Fig. 9. It was explained that the increase of pH value at the initial stage is due to the neutralization of the nitric acid by the ammonium hydroxide, and after the acid was neutralized the pH value reached a constant; while the slight decrease of the pH value in the last stage is due to the evaporation of ammonia, or to a CO_2 buffering effect [84]. Notably, the maximum pH value obtained from system containing SBA-15 is significantly lower than that obtained from blank system (without SBA-15). Considering that the surface of SBA-15 is rather inert, the decrease in the pH value could be due to a result of an interaction between the precipitating Pt species and the support [82], or to the formation of a metal phase that is more stable than the phase formed in the absence of the support [84].

Other than that prepared by WI method, the Pt/SBA-15 prepared by DP method (Pt/SBA-15_DP) showed systematic changes in relative to SBA-15 in N_2 adsorption–desorption isotherms, Fig. 4, such as expansion of mesopores, lowering of BET surface area, and tilt of hysteresis loop [85]. These changes indicated that part of the SBA-15 was transferred into amorphous non-ordered silicas [69], which was supposed to be due to the treatment in aqueous solution during the synthesis process [86].

However, no significant change in the small-angle XRD patterns (Fig. 5(A)) was observed between SBA-15 and Pt/SBA-15_DP, except a slight shift toward lower angle in the prominent XRD reflection

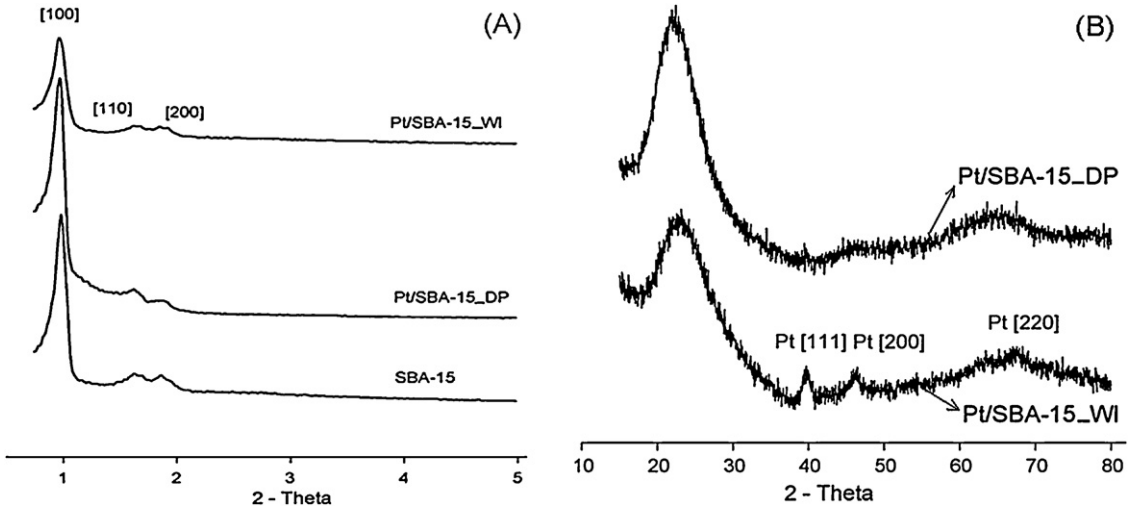

Fig. 5. X-ray diffraction patterns measured at small (A) and wide (B) angles for SBA-15 and Pt/SBA-15 prepared by WI and DP methods [69].

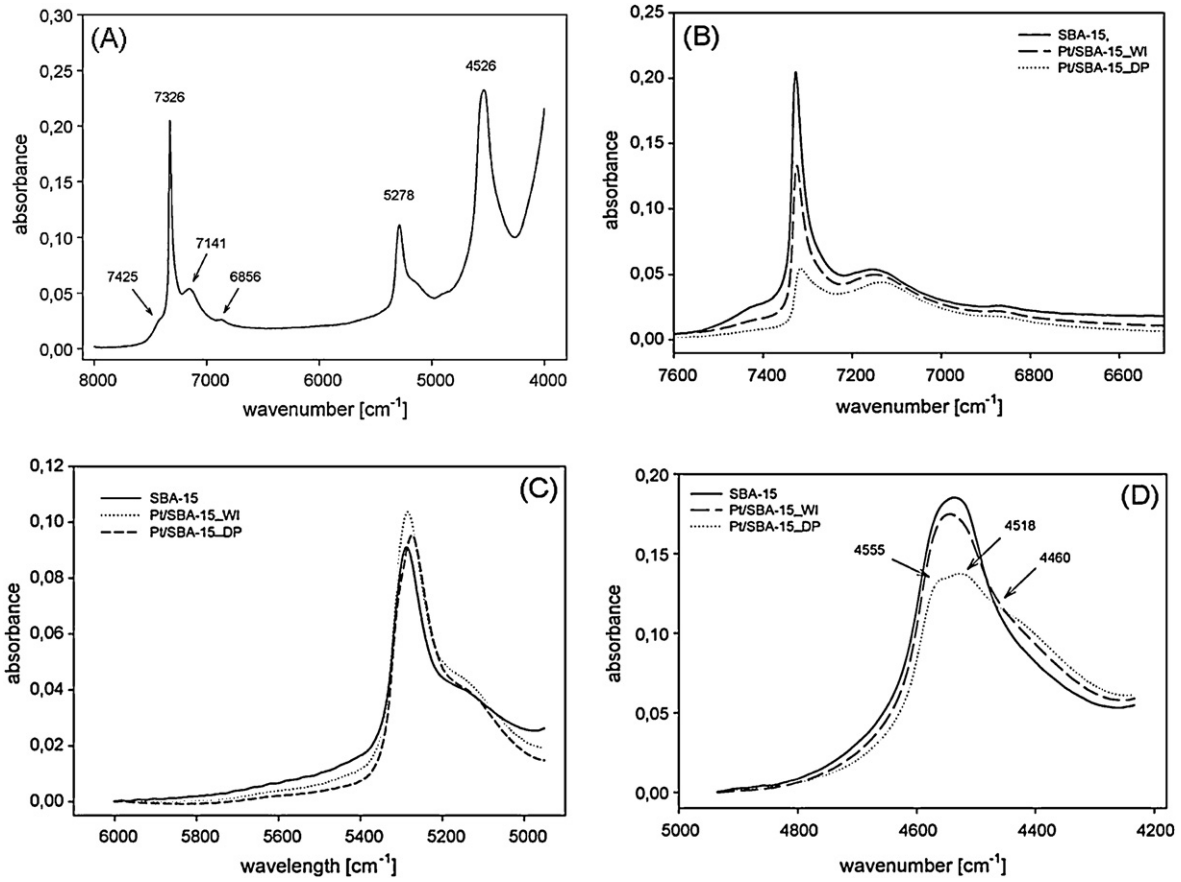

Fig. 6. Reflectance NIR spectrum of the first overtone region of SBA-15 (A), and those of SBA-15 and Pt/SBA-15 prepared by WI and DP methods at different ranges, (B)–(D) [69].

(1 0 0). This seems different from the conclusions derived from the N_2 adsorption–desorption measurement. The reason is that the XRD measurement detects only the preserved hexagonally ordered SBA-15, while the N_2 sorption occurs on the ordered SBA-15 as well as on the non-ordered amorphous silica [69]. Nevertheless, the estimation of the proportional amount of the ordered and non-ordered silica is almost not possible. These results also suggest that any data obtained from the combination of the XRD and N_2 adsorption–desorption measurements (e.g., the wall thickness) should be interpreted with some caution [69].

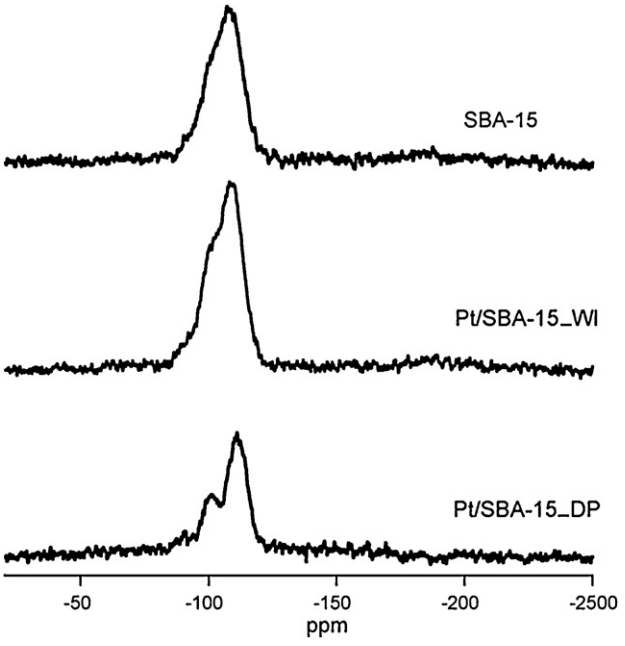

Fig. 7. ^{29}Si MAS NMR spectra of SBA-15 and Pt/SBA-15 prepared by WI and DP method [69].

No diffraction peak indexed to Pt was observed in the wide-angle XRD patterns of Pt/SBA-15_DP, Fig. 5(B), suggesting that either the Pt loading is too low to be detected, or the Pt particle size is below the detection threshold ($\leq$3 nm), or both. Also, it is found that compared to sample Pt/SBA-15_WI, the Pt/SBA-15_DP shows shaper diffraction peak at $2\theta = 23^\circ$ that is assigned to amorphous SiO_2 [87], suggesting that the silica framework of Pt/SBA-15_DP is more consolidated than that of Pt/SBA-15_WI.

Results from near-infrared (NIR) spectroscopy showed that the peak intensity of Pt/SBA-15_DP at 7326 cm^{-1} was significantly decreased comparing to that of SBA-15 and Pt/SBA-15_WI, Fig. 6, indicating a large amount of silanol was removed in Pt/SBA-15_DP [69]. Nevertheless, both Pt/SBA-15_WI and Pt/SBA-15_DP contained higher amount of water than SBA-15, as their peak intensity at 5270 cm^{-1} is stronger than that of SBA-15. Noticeably, the band at 4526 cm^{-1} for the Pt/SBA-15_DP was split into three components, as marked in Fig. 6(D). It was suggested that the band at 4555 cm^{-1} is attributed to the isolated SiOH groups, while those centered at 4518 and 4460 cm^{-1} are to SiOH groups hydrogen bonded to water molecules [69,71].

Decrease of silanols groups in Pt/SBA-15_DP was also evidenced by the ^{29}Si MAS NMR spectrum shown in Fig. 7. Other than those of SBA-15 and Pt/SBA-15_WI, the Q^n bands of Pt/SBA-15_DP were well distinguished and three definite peaks were observed, indicating that the material has better short-range order of the silica

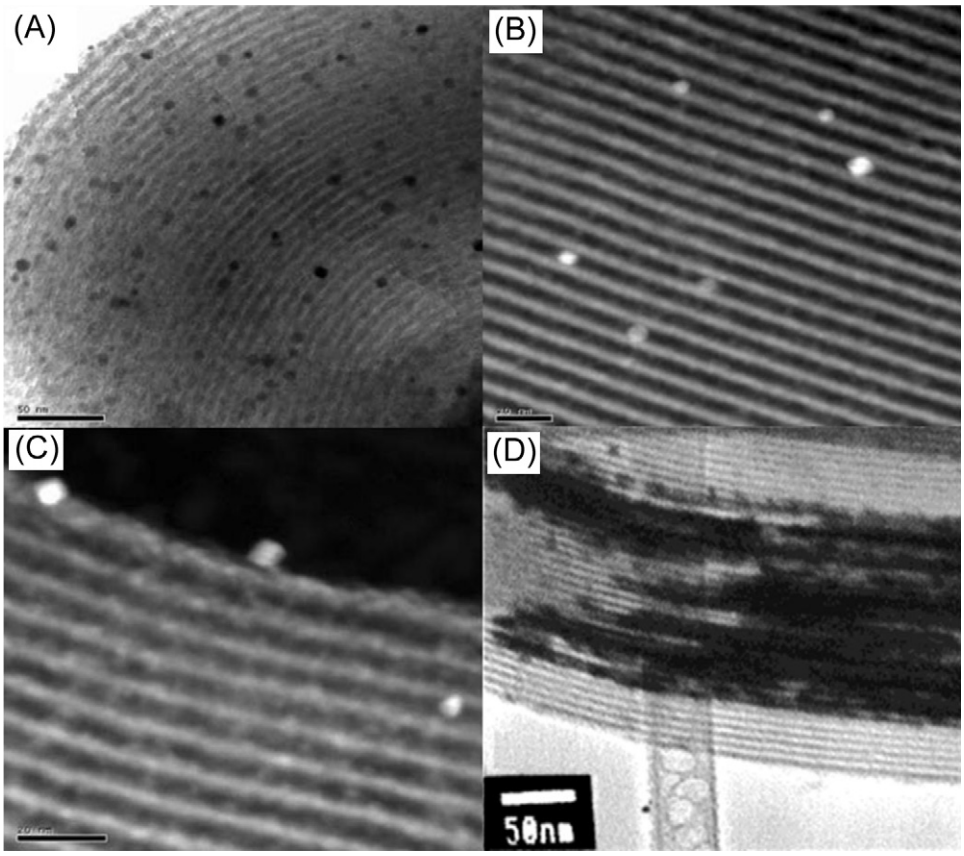

Fig. 8. TEM/STEM images of Pt/SBA-15 prepared by WI method [80,81].

framework. The improvement of the short-range periodicity in Pt/SBA-15_DP was proposed to be a consequence of the decrease in the number of silanols groups [69].

Despite of the formation of non-ordered amorphous silica in Pt/SBA-15_DP, well ordered SBA-15 structure was observed in the TEM images, Fig. 10. This indicates that although the aqueous solution has negative effect on the porous structure (see Fig. 4), a large fraction of SBA-15 could be maintained after the preparation process. The Pt particle size measured from the TEM images shows a wide size distribution, with the largest more than 15 nm, Fig. 10(B), and the smallest less than 2 nm, Fig. 10(C), suggesting that the Pt NPs can either be supported on the surface of SBA-15, or attached inside the pores of SBA-15.

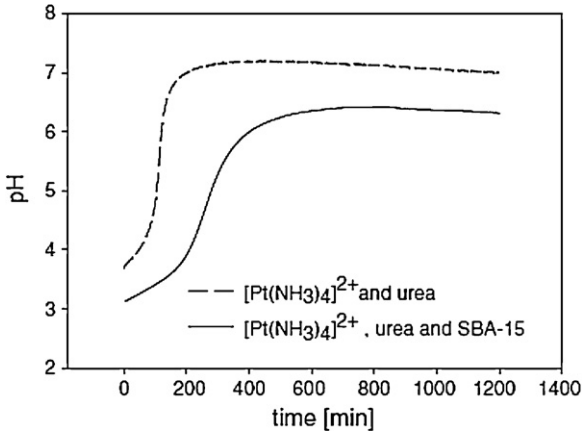

Fig. 9. Time dependent pH changes during the DP process as monitored for Pt on SBA-15 at 90 °C [80].

By comparison, it can be found that the Pt/SBA-15 prepared by DP method possesses smaller Pt particle size than that prepared by WI method. Besides, as a washing process was conducted in the DP method, most of foreign ions (e.g., Cl^-) brought from the Pt precursor (e.g., $H_2PtCl_6{\cdot}6H_2O$) can be removed and thus their effect on the subsequently catalytic reaction could be alleviated. However, the operation of DP method is complex and it needs careful attention on the time of the precipitant to be added, the pH value and the temperature used, and other conditions that could affect the morphology of the catalyst.

5. Pt/SBA-15 synthesized by graft hybrid (GH) method

Other than that in the WI and DP methods, in the GH method the deposition of metal ions on the support is through electrostatic interactions. Namely, the charged metal precursors in the solution were firstly absorbed and interacted with the oppositely charged organic groups functionalized in the pores or on the surface of the support, thereafter the sample was subjected to filtration, washing, drying and calcination to remove the organic functional groups and finally by a reduction process to reduce the metal ions. In the case of Pt/SBA-15, a procedure reported by Chao et al. [88] is as below: the synthesized SBA-15 was first pretreated in water for 1 h by refluxing, followed by heating in a vacuum at 150 °C to remove the residual water. The pretreated SBA-15 was then suspended in toluene, and the precursor of the functional group, N-trimethoxysilylpropyl-N,N,N-trimethylammonium chloride (TPTAC, 50 wt.% in methanol), was subsequently added. The mixture was stirred at room temperature for 12 h, followed by refluxing at 80 °C for 6 h. The obtained sample was washed with toluene and ethanol, and dried in air. Afterwards, the functionalized TPTAC-SBA-15 was mixed with the ethanol solution of H_2PtCl_6

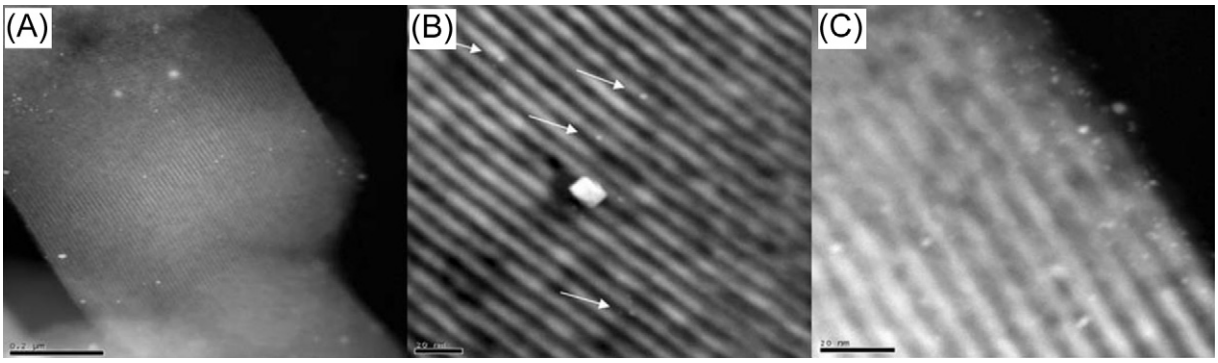

Fig. 10. STEM images of Pt/SBA-15 prepared by DP method (calcined in air at 300 °C for 2 h). All images taken in ADF STEM imaging mode [80].

to exchange the Pt^{4+} ions. After ca. 10 min, the solids were washed with ethanol, dried in ambient air, and finally reduced in hydrogen flow at 100–300 °C to yield product Pt/SBA-15_GH.

To confirm that the functional groups (i.e., TPTAC) were grafted on the pore surface of SBA-15, the authors [88] performed FTIR and ^{29}Si NMR measurements on the samples. The FTIR results indicated that the intensity of silanol groups at 3750 cm^{-1} for SBA-15 was decreased after the functionalization, accompanied with the appearance of absorption peaks of C—H bonds (2900–3000 cm^{-1}), C—N bonds (~1490 cm^{-1}), and Si—C bonds (~1250 cm^{-1}), confirming that the TPTAC was adsorbed on the surface of SBA-15. Results from ^{29}Si NMR spectra showed distinct resonances for siloxane [Q^n = Si—$(OSi)_n(OH)_{4-n}$, n = 2–4] and organosiloxane [T^m = R—Si—$(OSi)_m(OH)_{3-m}$, m = 1–3] in the functionalized SBA-15, Fig. 11. The ratio of Q^3 to Q^4 decreased from ca. 0.8 for the rehydrated SBA-15 to ca. 0.5 for the TPTAC treated sample, and accompanied with the appearance of T^2 and T^3 that assignable to the organosiloxane. This indicates that the amount of silanol groups are decreased and functionalized to organosiloxane groups due to the interaction between TPTAC and siloxane.

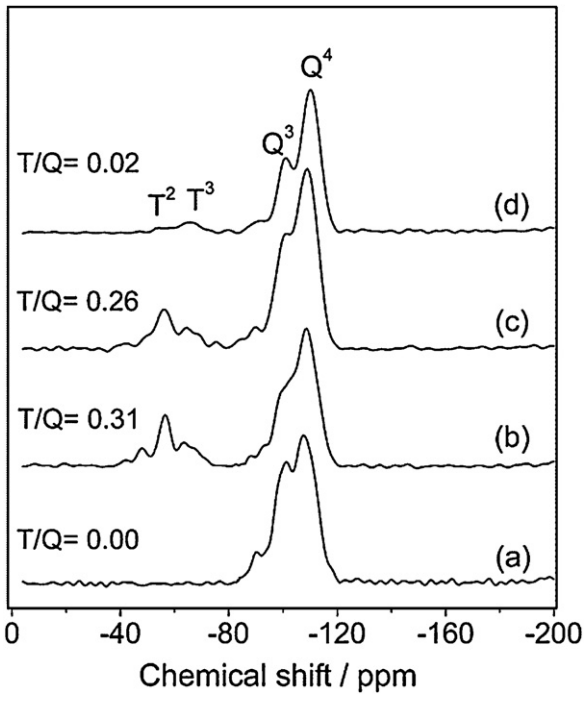

Fig. 11. ^{29}Si NMR spectra of rehydrated SBA-15 (a), TPTAC-SBA-15 (b), and Pt/SBA-15 reduced at 423 K (c) and 573 K (d), respectively [88].

Also, the T^m/Q^n ratio, which represents the incorporation amount of functional groups [88], decreased from 0.31 for TPTAC-SBA-15 to 0.26 for Pt/SBA-15 reduced (by H_2) at 150 °C, and further to 0.02 for Pt/SBA-15 reduced (by H_2) at 300 °C. This suggests that most of the surface functional groups remained after H_2 reduction at 150 °C, but were almost removed at 300 °C. The maintained surface functional groups at 150 °C suggest that they could be used for further metal incorporation processes. The removal of surface groups at 300 °C is in accordance to the results obtained from the thermal analysis of TPTAC-SBA-15 carried out under nitrogen flow [89].

The formation process of Pt/SBA-15_GH monitored by in situ XAS measurement showed that the white line intensity decreased and the shape of the absorption profile changed when the as-synthesized sample (Pt/SBA-15(s)) was reduced (by H_2) at 300 °C (Pt/SBA-15(r)), due to the decomposition of $PtCl_6^{2-}$ anions to Pt NPs, Fig. 12(A). The white line intensity increased slightly and the absorption edge shifted toward the standard platinum oxide when the reduced sample was exposed to air (Pt/SBA-15(a)), suggesting that part of Pt NPs has been oxidized.

Fourier transform profiles of K^3-weighted Pt L_{III}-edge EXAFS, Fig. 12(B), and the corresponding curve fitting results, Table 2, showed that Pt/SBA-15(s) consists of a single peak of Pt—Cl (d = 2.33 Å) with coordination number (CN) of 6, which is identical to that of H_2PtCl_6, suggesting that the $PtCl_6^{2-}$ anions were not perturbed in the Pt/SBA-15(s). After reduction, the profile contained mainly a first-shell Pt-Pt peak with d = 2.77 Å and CN = 10.3. The intensity of the Pt—Pt peak decreased and a new peak assigned to Pt—O band (d = 2.01 Å,CN = 1.0) appeared after the reduced sample was exposed to air, indicating that part of the metallic Pt were re-oxidized. Accordingly, the CN of Pt—Pt decreased from 10.3 to 7.5 and the particle size decreased from 2.9 to 1.0 nm (Table 2).

For the textural properties, N_2 adsorption–desorption isotherms, Fig. 13(A), and the corresponding pore size distribution, Fig. 13(B), showed that the surface area, the total pore volume as well as the pore size decreased significantly after the deposition of Pt NPs, suggesting that the pores of SBA-15 are blocked and/or the Pt NPs are attached on the channels of SBA-15. Whereas, the relatively large pore volume and pore size suggest that most of the pores are still available and can be used for further metal incorporation. The broadened hysteresis loops (in particular for the desorption branch) indicated that Pt/SBA-15_GH has wider pore size distribution (toward small pore size) than SBA-15, due to the attachment of Pt particles on the pore walls of SBA-15.

XRD patterns measured in the small-angle region showed no significant change in the diffraction peaks of SBA-15 and Pt/SBA-15_GH, Fig. 14(A), indicating that the ordered structure of SBA-15 is well maintained in Pt/SBA-15_GH. Whereas, a slight decrease in the peak intensity of the (1 1 0) and (2 0 0) reflections was observed, which could be due to the difference in the scattering contrasts of

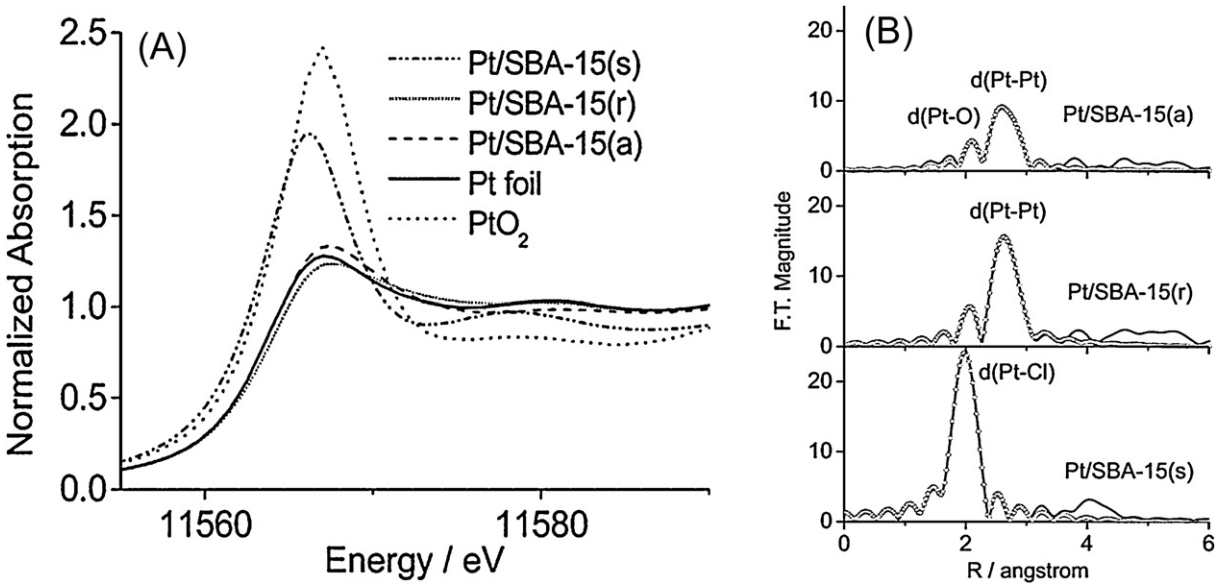

Fig. 12. (A) Normalized Pt L_{III}-edge XANES of Pt/SBA-15 samples (for meaning of the letters, please see the text), Pt foil, and PtO_2 powder. (B) Fourier transforms of Pt L_{III}-edge K^3-weighted EXAFS data (—) and the fitted results (○), respectively, for Pt/SBA-15 samples. Note that the phase shifts were not corrected [88].

Table 2
Pt L_{III}-edge EXAFS results for the in situ experiment of Pt/SBA-15 composite [88].

Sample	Shell	R (Å)[a]	CN[a]	σ^2 (10^{-3} Å^2)	R factor (10^{-4})	Particle size [b] (Nm)
Pt/SBA-15(s)	Pt—Cl	2.33	6.2	2.8	0.2	
Pt/SBA-15(r)	Pt—Pt	2.77	10.3	6.0	6.5	2.9
Pt/SBA-15(a)	Pt—Pt	2.77	7.5	7.1	27	1.0
	Pt—O	2.01	0.9	7.8		

[a] Interatomic distance and coordination number.
[b] Particle sizes were estimated from a spherical model with face-centered cubic Pt structure.

the pores and the walls, or to the formation of nanostructured Pt inside the channels of SBA-15, as that in the case of MCM-41 [89]. In the wide-angle region (Fig. 14(B)), the Pt/SBA-15_GH exhibits four broad and weak reflection peaks, which are assignable to Pt(1 1 1), (2 0 0), (2 2 0) and (3 1 1). The weak intensity and broad width of the reflection peaks suggest that Pt exists in nanocrystalline status, with very small particle size.

TEM images of the air-exposed Pt/SBA-15_GH in Fig. 15(A) showed that the Pt particles are highly dispersed and with uniform particle size (1.2–3 nm), and the Pt NPs are almost stayed inside the channels of SBA-15. The cross sectional image presented in Fig. 15(B) showed that the Pt NPs are disk-shaped, attaching on the hexagonal pore of SBA-15. It was suggested that the distinct shape of Pt NPs may derive from the electrostatic interaction between positively charged surface PTA groups and anionic Pt complexes, which tends to "pull" the reduced metal onto the pore surface of SBA-15 during reduction.

Shi et al. [90] also found that by selective functionalization of the SBA-15 support, Pt nanoclusters can be formed exclusively inside the pores. They first poisoned the external surface of SBA-15 by methyl group (SBA-CH_3), and then functionalized the internal surface of SBA-15 by hydrogen (SBA-H), to obtain an external methyl poisoned and internal hydrogen functionalized SBA-15. This material was used to graft the Pt^{4+} ions (from H_2PtCl_6 solution) under the

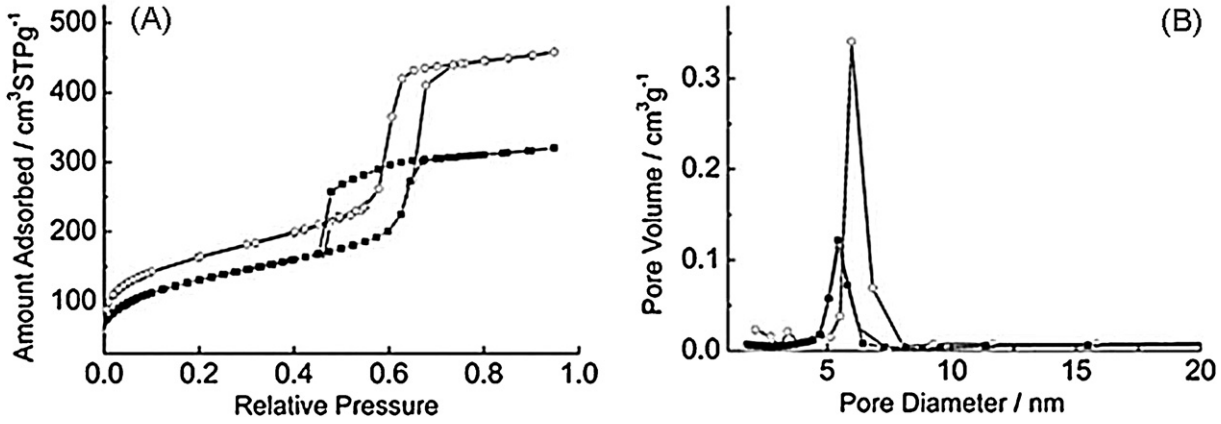

Fig. 13. (A) Nitrogen adsorption–desorption isotherms of calcined SBA-15 (○), Pt/SBA-15_GH (■). (B) Pore size distribution of the samples calculated from the desorption branch using the BJH algorithm [88].

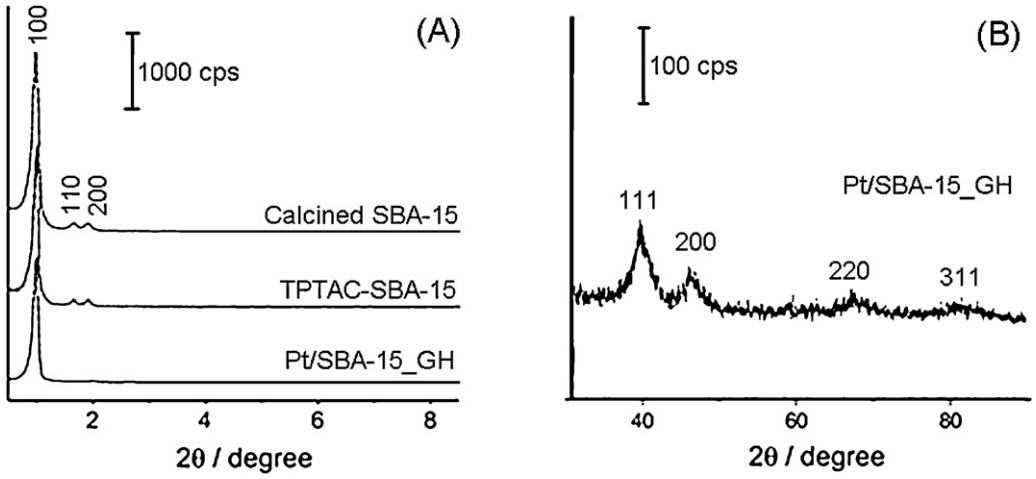

Fig. 14. (A) Small-angle PXRD of calcined SBA-15, TPTAC-SBA-15, and Pt/SBA-15 and (B) wide-angle PXRD of Pt/SBA-15 [88].

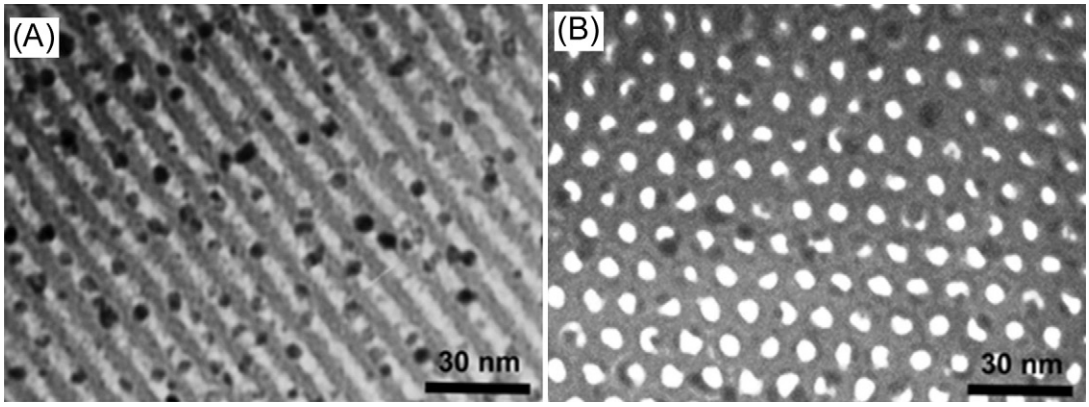

Fig. 15. TEM images of Pt/SBA-15 viewing normal to the pore axis (A) and along the pore axis (B) of host SBA-15 [88].

presence of CH_2Cl_2. The Pt^{4+} grafted SBA-15 was finally reduced by H_2 to obtain the SBA-15 supported Pt nanoclusters. Results of FTIR spectra (Fig. 16) of the poisoned and functionalized SBA-15 confirmed the presence of Si—CH_3 and Si—H groups, and TEM images showed that the Pt nanoclusters were formed inside the pores, Fig. 17. These results suggest that the Pt existing status in Pt/SBA-15_GH can be well controlled by selective functionalization of the SBA-15 support.

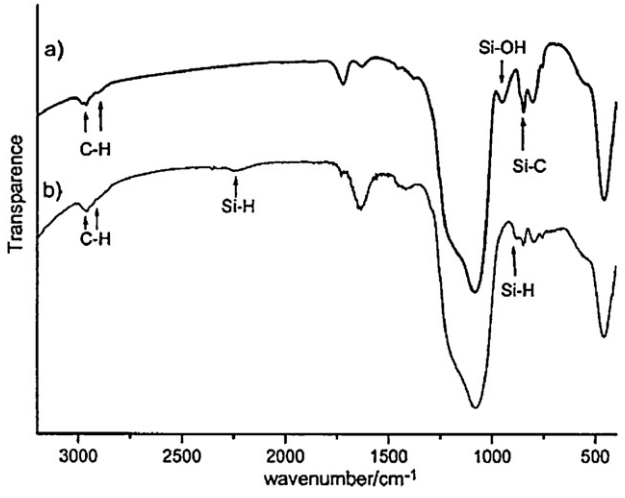

Fig. 16. FTIR spectra of (a) SBA-CH_3 and (b) SBA-H [90].

The advantages of this method is that the amount of organic groups functionalized on the SBA-15 can be easily controlled through changing the precursor and its amount, thus the pore structure of the SBA-15, the metal loading, as well as the morphology of the metal nanostructures can be tuned according to the specific needs. Also, as this method does not require the precipitation process, the metal ions can be highly dispersed on the support. However, it should be noted that the removal of the surface functional groups usually need extra treatment steps, e.g., high temperature calcination, which would lead to aggregation of the Pt NPs.

6. Pt/SBA-15 synthesized by colloid immobilization (CI) method

The CI method provides an attracting route for the preparation of NPs that are close to or smaller than 1 nm [91]. In this method, dendrimer encapsulated metal NPs were first synthesized, and then immobilized on the support by electrostatic and/or hydrogen bonding interactions between the dendrimers and the support [92]. The role of dendrimers serves not only as internal cavities for NPs growth, but also a shell to stabilize the NPs and to prevent aggregation of the as-grown NPs [93]. The synthesis procedure of Pt/SBA-15 by CI method is briefly described in Scheme 3. First, the Pt^{4+} ions from K_2PtCl_4 solution were interacted and encapsulated in a suitable dendrimer (e.g., Generation 4, G4OH), and the resulting K_2PtCl_4/G4OH solution was subsequently reduced by freshly prepared $NaBH_4$ solution to yield encapsulated Pt NPs,

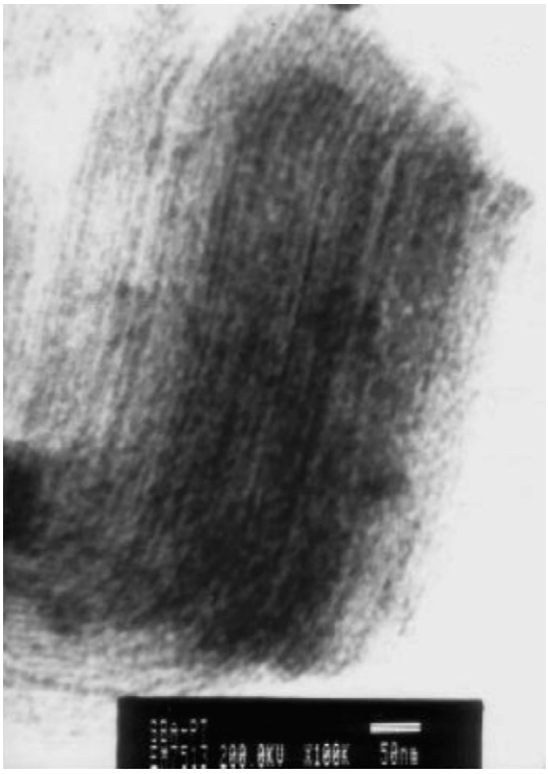

Fig. 17. TEM images of Pt-SBA showing the preferred growth of Pt nanowires along the pore channels [90].

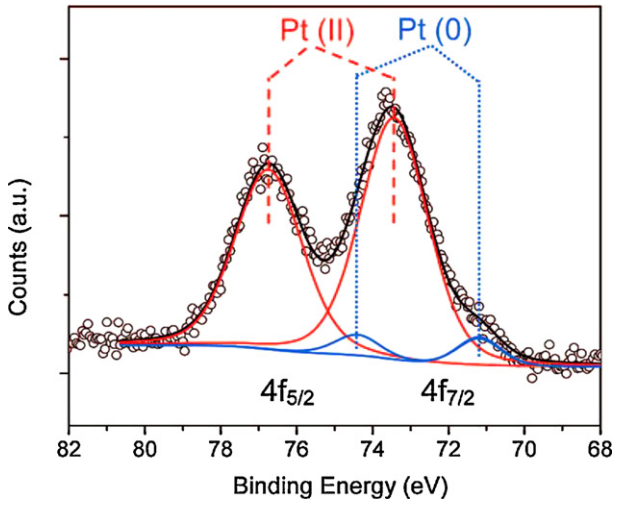

Fig. 18. X-ray photoelectron spectra of dendrimer encapsulated Pt_{20} NPs. Almost 93% of the Pt was oxidized for the Pt NPs [91].

which was thereafter immobilized on the SBA-15 support in an ultrasonic cleaner. Finally, the Pt NPs loaded SBA-15 was separated from solution by centrifuging, and the resulting slurry was subjected to drying to yield sample Pt/SBA-15_CI [91]. The separation of sample from solution using Rotavap system (to remove water) is also feasible [94].

In the reduction of Pt^{4+} ions, borohydride (BH_4^-) was proposed to be the most suitable reducing agent in minimizing the particle size comparing to hydrogen [95,96], alcohols [87,97], glycol [95,98] or ethylene glycol [99,100], as it enables rapid reduction to afford very small nuclei, whose growth is hindered. However, the Pt NPs yield is very low due to the incomplete reduction of the precursor ions [101–104], it is therefore essential to confirm how much Pt^{4+} ions were reduced to metallic Pt NPs. For this, X-ray photoelectron spectroscopy (XPS) technology would be useful as it is a powerful means in detecting the oxidation state of surface ions. Fig. 18 shows the XPS results of Pt NPs reduced by $NaBH_4$, reported by Somorjai et al. [91] The main Pt $4f_{7/2}$ peak of Pt NPs located at a binding energy of 73.5 eV, which is higher than that for metallic Pt (71.2 eV), suggesting that most of the Pt ions are not reduced. Deconvolution on the Pt $4f_{7/2}$ peak showed only ~7% of metallic Pt existed on the surface. Other authors [105–107] also found that the complete reduction of Pt^{4+} by $NaBH_4$ is not possible.

As expected, TEM image showed that Pt/SBA-15_CI remained the ordered mesorporous structure of SBA-15, and very small Pt particles were formed, Fig. 19, supporting that BH_4^- is a good reducing agent in preparing small Pt particles [91]. Because of the small particle size, accurate measurement on the Pt particle size is difficult, as TEM images taken from NPs loaded onto 3D supports often suffer from low contrast due to the decrease of the supporting material's

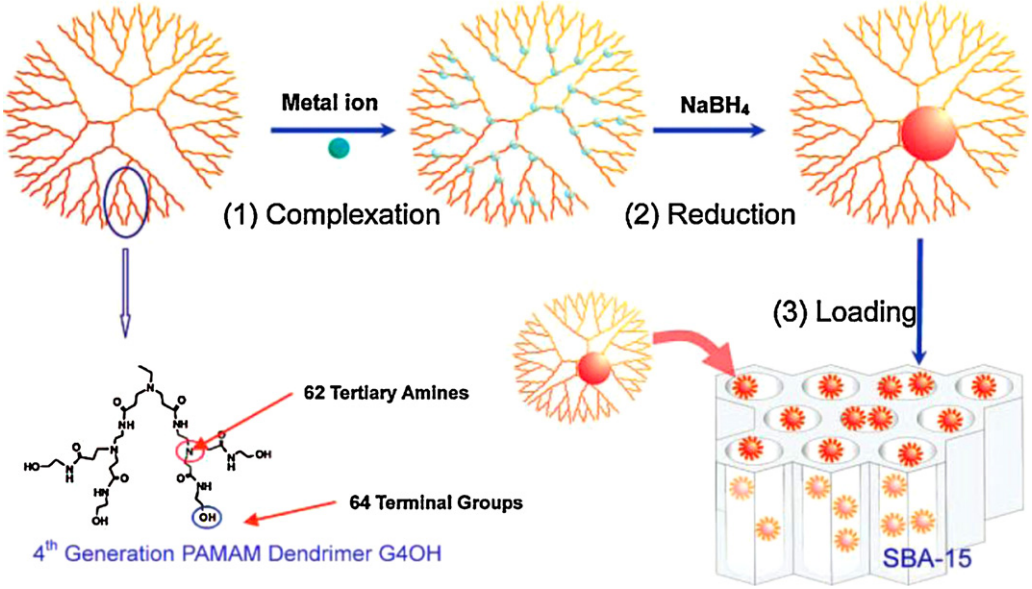

Scheme 3. Synthesis of dendrimer encapsulated metal NPs and the subsequent immobilization of the NPs on mesoporous SBA-15 support [91].

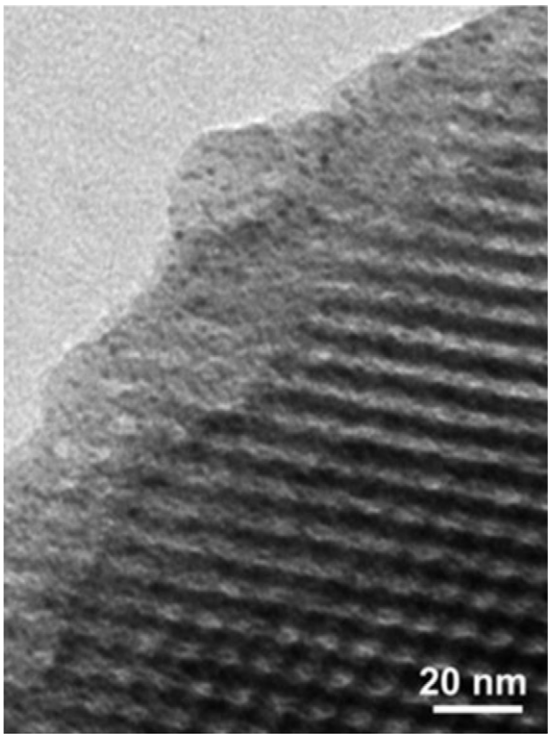

Fig. 19. TEM images of dendrimer encapsulated Pt_{40} NPs immobilized on SBA-15 [91].

electron transparency, and this behavior is magnified as particle size decreases [91].

One thing needs to be pointed out is that the Pt NPs can be expediently controlled as they were prepared before loading on the SBA-15 support and no drastic reaction occurred during the loading process, thus very small Pt particles could be prepared. For instance, Somorjai et al. [91] reported that Pt/SBA-15 with Pt particle size as small as 1.7 nm could be prepared using the CI method. Also, the authors found that the dendrimer encapsulated Pt NPs supported on SBA-15 is different from metal particles supported on other materials (e.g., Al_2O_3 [108,109], TiO_2 [110,111]), they were active for catalytic reaction even the dendrimer was not removed, due to the unique properties of the SBA-15 possessed. However, as the dendrimer encapsulated Pt NPs were simply loaded on the SBA-15 and the dendrimer was not removed, interaction between the Pt NPs and the SBA-15 support is weak and the Pt NPs are easy to leach if the catalyst is conducted in liquid phase reaction, resulting in unstable activity and short catalyst's life. Furthermore, the presence of dendrimer would block the pores of SBA-15, leading to low surface area and narrow pore size. This would reduce the catalytic performances of the Pt/SBA-15_CI catalyst when used for reactions that depend intimately on surface area and/or pore size.

7. Pt/SBA-15 synthesized by nanoparticle encapsulation (NE) method

The NE method, sometimes also called inclusion method [112], has similar synthesis procedure as that for the CI method, except that the Pt colloids were added during the synthesis process of SBA-15 and the Pt particles were in situ incorporated into the SBA-15 material, as illustrated in Scheme 4. Briefly, a dendrimer was first added to H_2PtCl_6 aqueous solution to cap or encapsulate the Pt^{4+} ions, which was then reduced by bubbling hydrogen gas for some time to yield the Pt NPs. The freshly prepared Pt sols were added to a solution containing triblock copolymer Pluronic P123, HCl and

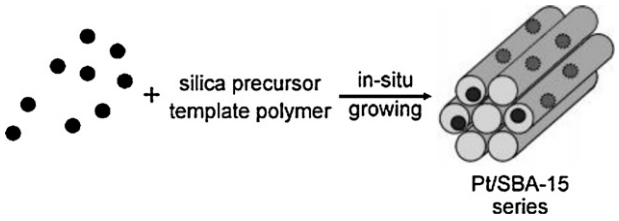

Scheme 4. Schematic of nanoparticle encapsulation (NE) method for the synthesis of Pt/SBA-15 [116].

tetraethoxysilane (TEOS) to obtain the Pt-containing sample, with the same treating procedures as that for SBA-15 [112–117].

Presence of Pt colloids in the synthesis process does not interfere with the formation of SBA-15, and the in situ synthesized Pt/SBA-15_NE shows ordered mesoporous structure as that of SBA-15, as evidenced by XRD patterns, N_2 adsorption–desorption isotherms and TEM images, Fig. 20 [116]. Further studies indicated that for Pt/SBA-15_NE synthesized using different Pt particle size, only the one with Pt particle size above 7.1 nm shows obvious diffraction peaks at $2\theta = 45.9^\circ$, 54.0° and 80.1° that assigned to the (1 1 1), (2 0 0), (2 2 0) reflections of the Pt fcc lattice in the XRD patterns, Fig. 20(A). This could be that the Pt particle in other samples is too small (below 7.1 nm) to be detected. Furthermore, it was found that the peak intensity of (1 0 0), (1 1 0) and (2 0 0) face observed from Pt/SBA-15_NE is stronger than that from the pure SBA-15, Fig. 20(B), suggesting that the presence of Pt NPs enhances the ordering of the hexagonal structure of SBA-15.

Similar as what observed in the above mentioned methods, although the mesoporous structure remained unchanged, the BET surface area and the pore volume of Pt/SBA-15_NE were significantly decreased compared to those of SBA-15, Fig. 20(C). The BET surface area of SBA-15 was decreased from 619 m^2/g to, for example, 545 m^2/g for 0.62% Pt (7.1 nm)/SBA-15, and the pore volume decreased from 2.05 cm^3/g to 1.65 cm^3/g.

Interestingly, the authors [116] found that the size distribution of the Pt NPs encapsulated in SBA-15 was almost unchanged compared to that of the Pt colloids. That is, the Pt particles were isolated and randomly distributed throughout the entire SBA-15 framework without severe agglomeration, Fig. 20(D), suggesting that the Pt NPs has high stability and that the Pt particle size is pre-determined in the preparation of Pt colloids step. Overall, the results indicated that Pt NPs can be incorporated into and well dispersed in the SBA-15 framework by an in situ route, without additional step to synthesize SBA-15 separately.

Besides the characterizations made in static status, the authors [116] also investigated the infrared spectroscopic measurements of CO adsorption on the series Pt/SBA-15_NE made in dynamic status. Results showed that atop-bonded CO was the dominant interaction between CO and the Pt surface, and no bridge-bonded CO appeared, Fig. 21. Significantly, the frequency of the adsorbed CO depended on the Pt particle size, and the position of the atop frequency red-shifted by $\sim$15 cm^{-1} from the 1.7 to 7.1 nm particles, suggesting that CO is a good probe molecule in assessing the status of the Pt surface. Similar phenomena have also been observed elsewhere [118,119]. This suggests that the strength of π back-donation of the CO chemisorption bond is stronger on smaller particles with a large fraction of low-coordination metal sites than that on single crystal or Pt particle with a large fraction of high-coordination surface sites.

We recently found that when Pt/SBA-15_NE was prepared using poly(vinyl alcohol) (PVA) as protecting agent and $NaBH_4$ as the reducing agent of Pt colloids [60,64], the obtained sample not only showed the ordered structure as that of pure SBA-15, but also exhibited enhanced BET surface area and unchanged pore size,

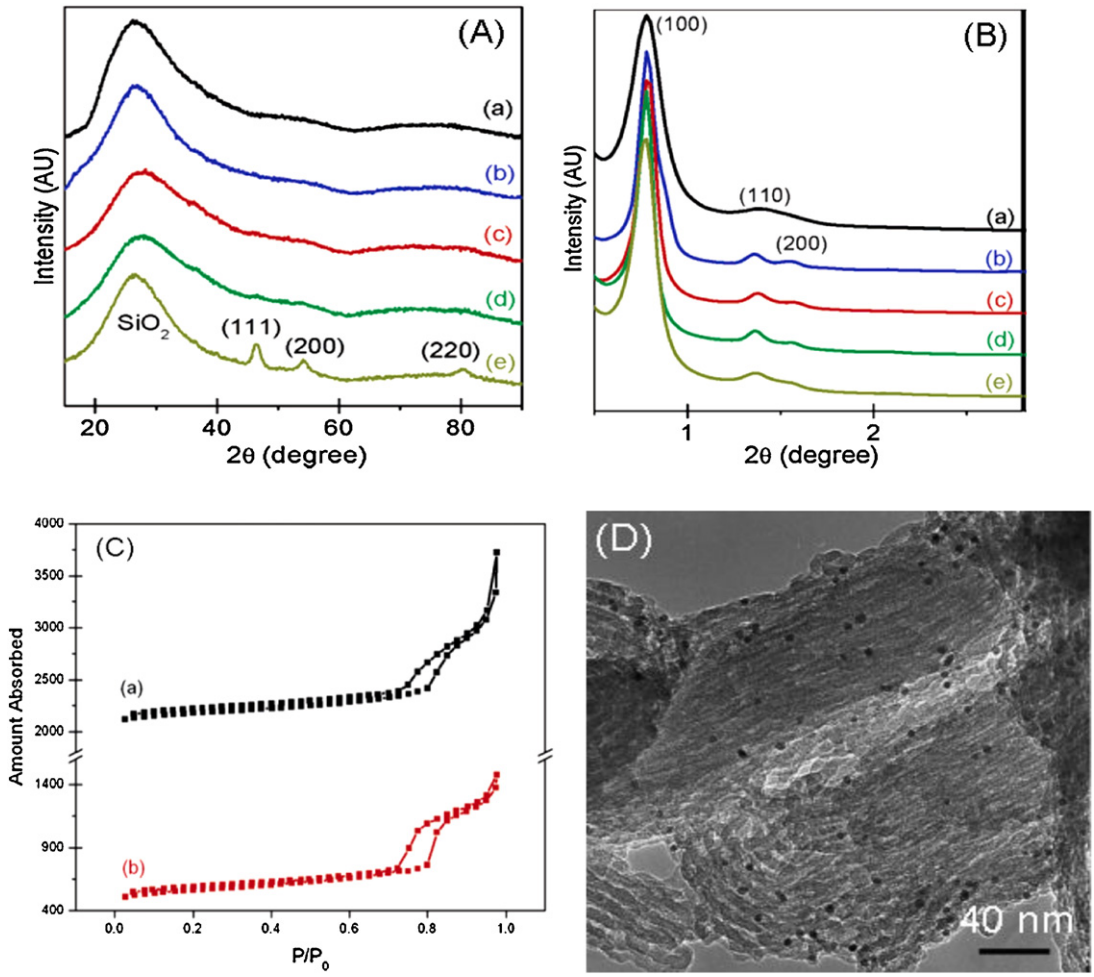

Fig. 20. (A) XRD and (B) SXAS data for (a) SBA-15 and Pt(*X*)/SBA-15 catalysts, *X* = (b) 1.7 nm, (c) 2.9 nm, (d) 3.6 nm, and (e) 7.1 nm. In (A), the Pt(1 1 1), Pt(1 1 0), and Pt(2 0 0) peaks of the fcc lattice are indicated for Pt (7.1 nm)/SBA-15; In (B) the SBA-15 (1 0 0), (1 1 0), and (2 0 0) peaks are indicated, demonstrating the long-range order of the channels. (C) N_2 adsorption–desorption isotherms of (a) SBA-15 and (b) 0.77% Pt (2.9 nm)/SBA-15 catalysts. Isotherms for the other catalysts look similar and are therefore not included. The hysteresis loop observed is indicative of cylindrical pores. (D) TEM images of Pt (2.9 nm)/SBA-15 catalysts. The curves in (A)–(C) are offset for clarity [116].

despite the amount of Pt was added (Fig. 22(A)–(D)). This is totally different from results described above, in which the BET surface area and/or the pore size of SBA-15 were significantly decreased after the deposition of Pt NPs. The average Pt particle size was evaluated to be 9.3 nm, similar to the pore size of the SBA-15 support (ca. 9.5 nm), thus the Pt particles can either be attached on the external surface or in the internal pore wall of SBA-15. Detailed studies [60] indicated that the PVA itself has the ability to create pores in silica (no P123 added this time), Fig. 22(E), and additional pores were created in the PVA assisted SBA-15 (denoted as SBA-15_PVA, Fig. 22(F)). Consequently, we considered that the enhanced BET surface area of Pt/SBA-15_NE is due to the new pores created by removing the PVA, as illustrated in Scheme 1. These results indicate that PVA is a good copolymer in preparing SBA-15 supported metal NPs with high surface area and large pore size. This is very useful especially when Pt/SBA-15 is used as catalyst for reactions that depend closely on the surface area and pore size of catalyst.

8. Catalytic applications

8.1. CO oxidation

CO is one component of exhaust emitted from industrial devices consuming fossil fuels, such as cars and power plants, and the removal of CO receives great attention especially after the issue of legislation on the exhaust emission. On the other hand, because of the simplicity of the reaction, CO oxidation is also widely used as testing reaction to evaluate catalytic performances of catalysts. Consequently, catalytic activities of CO oxidation over Pt/SBA-15 were investigated [120,121], to evaluate the catalytic performances of Pt/SBA-15, and also to check if Pt/SBA-15 has the possibility of being used as an industrial catalyst for CO removal.

Fig. 23(A) shows the catalytic activities of CO oxidation carried out over Pt/SBA-15 with various Pt loading (synthesized by NE method) as a function of reaction temperature [60]. For a given conversion, the reaction temperature decreased with the increase of Pt loading, showing that the increase of Pt amount favors the reaction to proceed. A big increase in the activity was observed from $Pt_{0.03}$/SBA-15 to $Pt_{0.1}$/SBA-15 (means the Pt loading is 0.03 and 0.1 wt.%, respectively. The same meaning for other samples), while the increase in the activity is small for catalysts with higher Pt loading ($\geq$0.1 wt.%). This indicates that the surface Pt sites that are active for CO oxidation is not in scale to the total Pt amounts. One possible reason could be that part of the Pt NPs was encapsulated in the silica framework, and the scale of the encapsulated Pt NPs varied with the total Pt amounts. Thus for $Pt_{0.03}$/SBA-15, the low activity is due to its extremely low Pt loading and that some of the Pt particles were encapsulated in the SBA-15, leading to very few Pt particles on the surface to catalyze the CO oxidation reaction. Indeed, the Pt element was even not detected in the

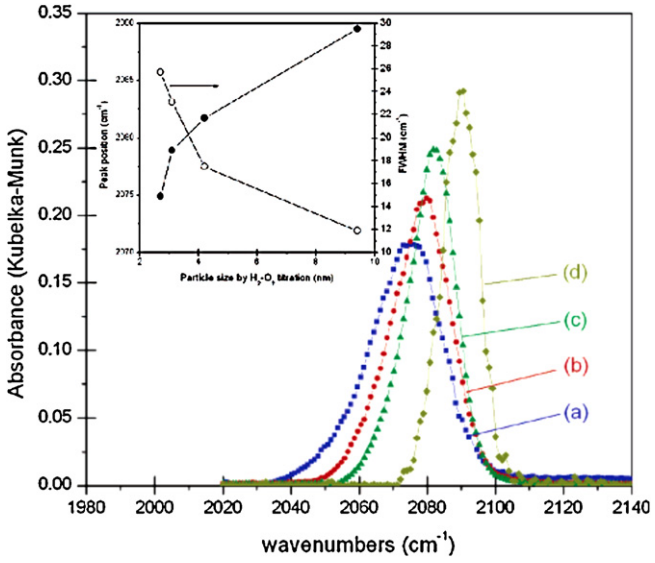

Fig. 21. Infrared spectrum of CO adsorption at 295 K for the Pt/SBA-15 catalyst series: (a) 2.33% Pt (1.7 nm)/SBA-15, (b) 2.69% Pt (2.9 nm)/SBA-15, (c) 2.62% Pt (3.6 nm)/SBA-15, and (d) 2.86% Pt (7.1 nm)/SBA-15. Inset is the peak position and FWHM of the atop CO stretching vibration as a function of particle size at room temperature. At saturation coverage, the peak position red-shifts due to changes in the average coordination number as the particle decreases. Peak heights have been modified for clarity [116].

XPS measurements, Fig. 23(B), which shows significant decrease in the Pt peak intensity with the decrease of Pt loading. The small increase in the activity of catalysts with high Pt loading (≥0.1 wt.%) may be explained that the amount of surface Pt particles is efficient to catalyze CO oxidation under the reaction conditions even for $Pt_{0.1}$/SBA-15, hence only a small increase in the activity was observed. The ignition temperature (~300 °C) of the Pt/SBA-15 for CO oxidation is in agreement with that of Pt/$mSiO_2$ reported by Somorjai et al. [117] Turnover frequency (TOF) of the Pt/SBA-15 for CO oxidation however indicated that the activity decreased with the increase of Pt loading, Fig. 23(C), confirming that the amount of valid Pt (used for CO oxidation) is not scaled with the Pt loading, as suggested above. Long-time stability test (Fig. 23(D)) and TEM images (Fig. 23(E) and (F)) showed that the catalyst has stable activity for CO oxidation even after running for at least 14 h, and the Pt NPs have strong resistance to aggregation even were treated at 300 °C, suggesting that the Pt/SBA-15 prepared by NE method has high thermal stability, and is a good catalyst for CO oxidation carried out at high temperature.

8.2. Toluene hydrogenation

Aromatics hydrogenation is a structure insensitive reaction [122], and vapor-phase toluene hydrogenation is regarded to be a good tool to characterize the number and nature of accessible supported metal atoms [123,124], although the support can contribute to the reaction if it is acidic [123,125]. For Pt/SBA-15, of which the support SBA-15 is non-acidic, this reaction can be exclusively used as a measure of the accessible Pt atoms.

Table 3 lists the activity of toluene hydrogenation carried out over Pt/SBA-15 that were prepared by NE (Pt_{nano}/SBA-15) and WI ($Pt_{0.1}$/SBA-15) method, with 1 wt.% Pt loading [112]. Both samples were active for the reaction and gave only methylcyclohexane as the product. Either the apparent activity or the intrinsic TOF values of Pt_{nano}/SBA-15 was lower than that of $Pt_{0.1}$/SBA-15, suggesting that the Pt/SBA-15 prepared by WI method is better than that prepared by NE method when used for toluene hydrogenation. H_2 chemisorption data (Table 3) indicated that $Pt_{0.1}$/SBA-15 has better Pt dispersion than Pt_{nano}/SBA-15. Together with the catalytic activity and the H_2 chemisorption results, it was suggested that the available and catalytically active Pt surface is represented by the total H_2 chemsorption, and the lower activity of Pt_{nano}/SBA-15 is that some of Pt atoms were covered by a residue of the copolymer or embedded in the silica, decreasing the Pt surface.

8.3. Propane dehydrogenation

Pt/SBA-15 can be a catalyst not only for hydrogenation reactions, but also for dehydrogenation reactions. As an example, dehydrogenation of propane, which has the potential to make up the shortfall of propylene supply left by conventional crackers, has been investigated by many authors using Pt/SBA-15 as catalyst [126–128]. In this reaction, besides the dehydrogenation reaction to C_3H_6, cracking reaction to C_1, C_2 products and even coking reaction to surface carbon are possible. This requires the catalyst is not only active for propane conversion, but also highly selective to C_3H_6 formation.

Kumar et al. [22] have investigated and compared the catalytic performances of Pt/SBA-15_WI and Pt/SBA-15_DP for dehydrogenation of propane. Table 4 lists the characters of Pt particle size of the two catalysts, measured from TEM, XRD and H_2 chemisorption, which shows that the Pt particles of Pt/SBA-15_DP are far smaller than that of Pt/SBA-15_WI, and hence suggests that the DP method is more favorable for the preparation of small Pt particles than the WI method. Catalytic results showed that the Pt/SBA-15_DP has higher initial C_3H_8 conversion than Pt/SBA-15_WI, Fig. 24(A), but low initial selectivity to C_3H_6 (40% vs. ~90%), Fig. 24(B). The most significant effect of the Pt particle size is on the coke formation. Large amounts of coke were formed over Pt/SBA-15_DP, while no obvious coke was observed over Pt/SBA-15_WI (Fig. 24(A)). These results indicated that small Pt particles are active for C—C bond activation, while large Pt particles are selective for C—H bond activation, as has also been reported by other authors [87,129].

Dependence of activity on the reaction time showed that for Pt/SBA-15_DP, C_3H_8 conversion decreased and selectivity to C_3H_6 increased after a few minutes on stream. This was explained that the coke formed during the reaction improved the selectivity by deactivating the Pt sites that are highly active for C—C bond activation [22]. While for Pt/SBA-15_WI, both C_3H_8 conversion and selectivity to C_3H_6 decreased with the time on stream, due to the rearrangement or modifications in the behavior of Pt particles during the reaction [130]. Nevertheless, activity with respective to the surface Pt sites (TOF) was lower on Pt/SBA-15_DP than that on Pt/SBA-15_WI (Table 4). The reason was supposed to be that the true initial TOF is difficult to determine over the former due to rapid deactivation of Pt sites by coke [22].

8.4. Catalytic oxidation of volatile organic compounds (VOCs)

Volatile organic compounds (VOCs) emitted from industrial plants are one class of major contributors to air pollution and are dangerous to human health [131]. Catalytic oxidation is one of the most efficient ways of removing VOCs, since VOCs oxidation over a catalyst takes place at temperature much lower than those required for thermal decomposition [132].

As one member of VOCs, polycyclic aromatic hydrocarbons (PAHs), which are emitted from diesel engines, are ubiquitous carcinogenic substances to which humans are exposed from the environment [133]. They are listed as carcinogenic and mutagenic priority pollutants, belonging to the environmental endocrine disrupters, and therefore the elimination of PAHs in the sources is one of the priority and emerging challenges.

Park et al. [134] studied the catalytic performances of Pt/SBA-15 (prepared by WI method) for the oxidation removal of PAHs.

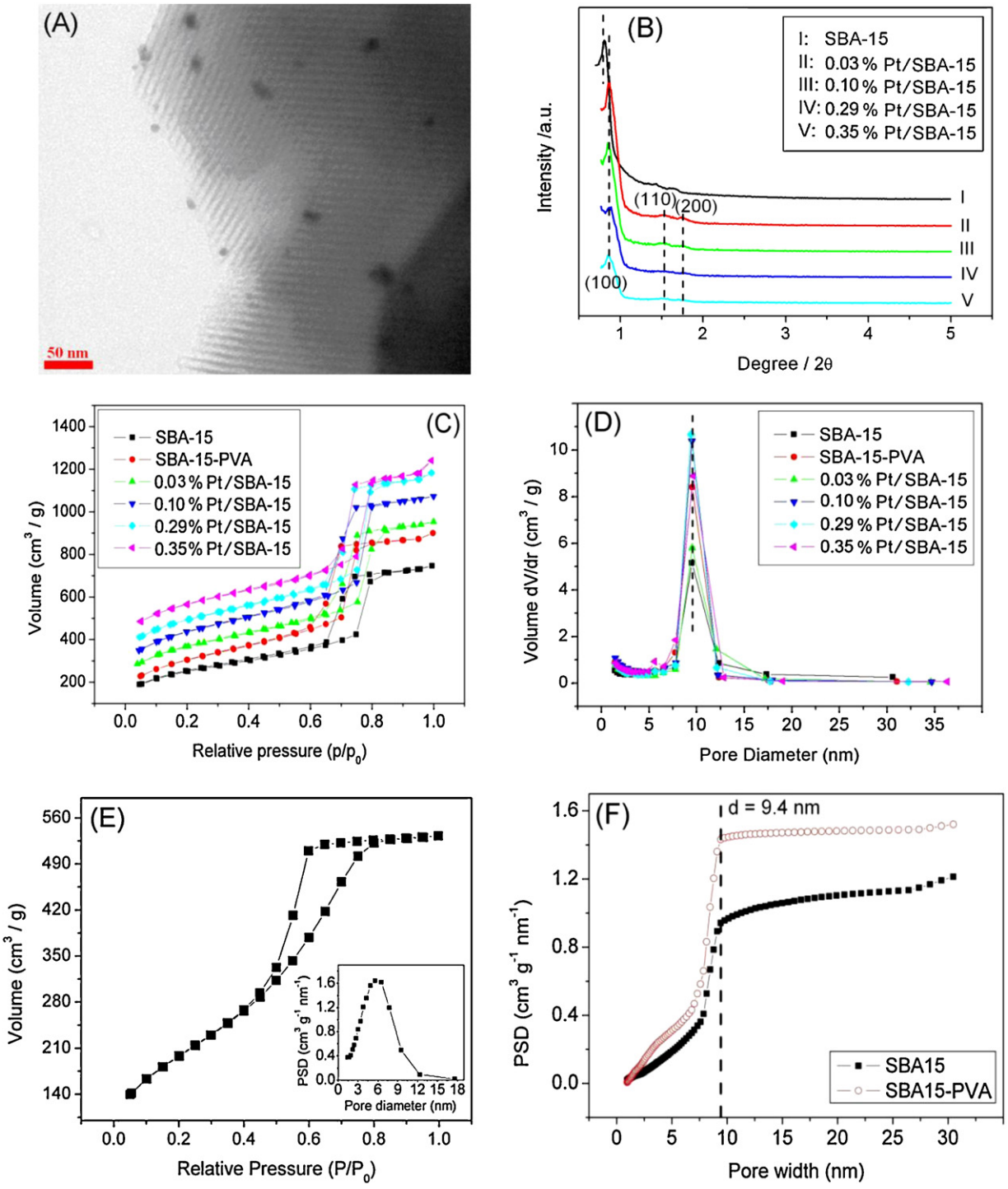

Fig. 22. (A) TEM images of Pt/SBA-15_NE with Pt loading of 0.29 wt.%; (B) small angle X-ray scattering (SAXS) of pure SBA-15 and that after incorporation of various amounts of Pt; (C) N_2 adsorption–desorption isotherms and (D) pore size distributions of pure SBA-15 and that after addition of PVA and various Pt contents; (E) N_2 adsorption–desorption isotherms for PVA templated silica and the corresponding pore distribution (insert); (F) cumulative pore volume for SBA-15 and SBA-15-PVA (obtained using the NLDFT method) [60,64].

Table 3
Activity in toluene hydrogenation and H_2 chemisorption results of Pt_{nano}/SBA-15 and $Pt_{0.1}$/SBA-15 [112].

Catalyst	H_2 chemisorption		Activity (μmol g^{-1} s^{-1})[a]	TOF (s^{-1})
	Dispersion (%)	Particle size (nm)		
Pt_{nano}/SBA-15	8.0	14.1	2.1	0.051
$Pt_{0.1}$/SBA-15	24.6	4.7	8.5	0.067

[a] Reaction rate for toluene conversion. Conditions: toluene WHSV 12.5 h^{-1}, H_2/toluene 40, 240 °C, 10 bar.

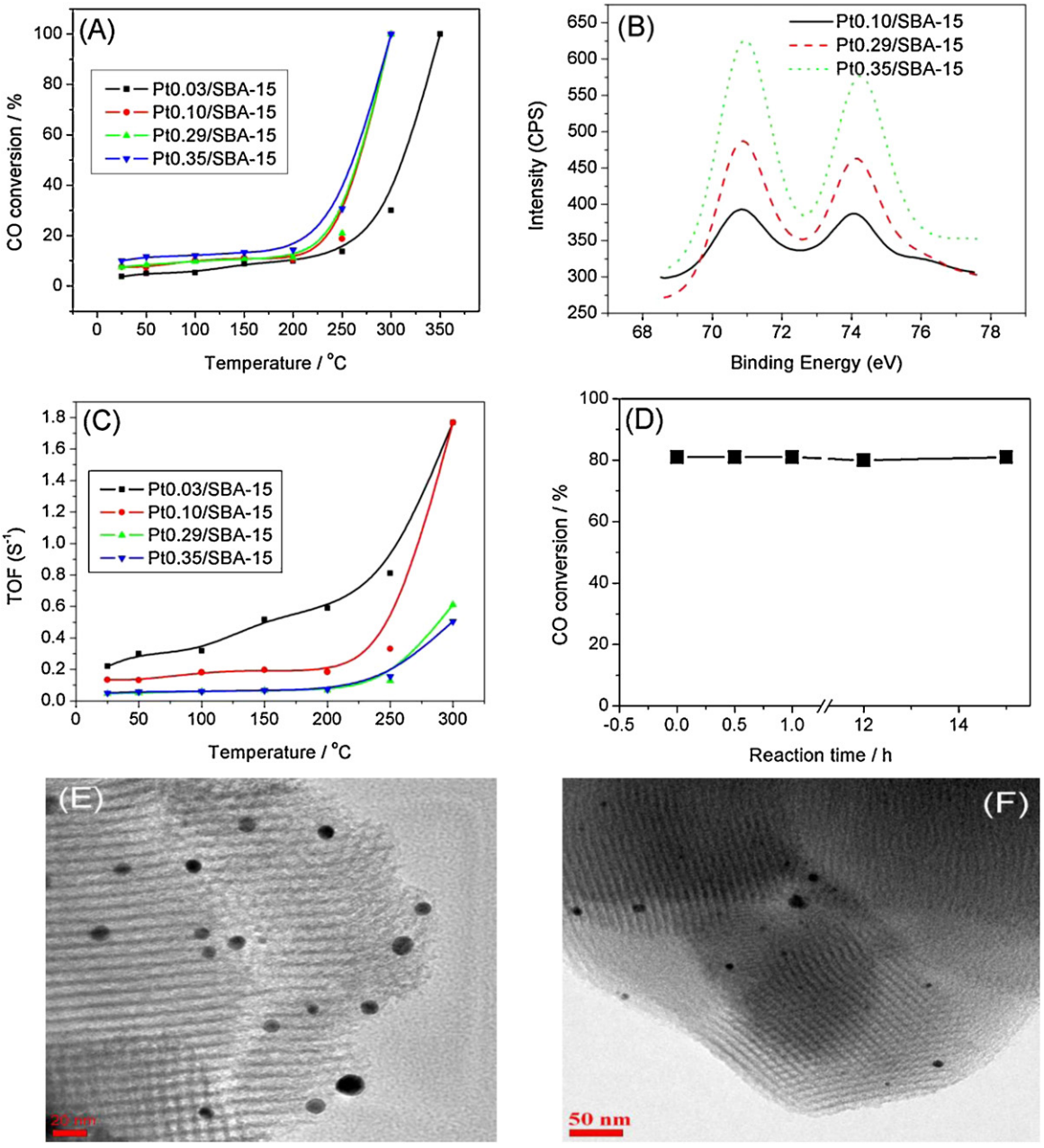

Fig. 23. (A) Dependence of CO conversion on the reaction temperature over the series of Pt/SBA-15; (B) high resolution XPS spectra of the series Pt/SBA-15 catalysts in the Pt 4f regions (no Pt element was detected over $Pt_{0.03}$/SBA-15 and its spectra was not shown); (C) dependence of CO TOF on the reaction temperature over the series of Pt/SBA-15; (D) long-time stability test for $Pt_{0.1}$/SBA-15 in CO oxidation at 290 °C; (E) and (F) TEM images of $Pt_{0.1}$/SBA-15 before and after CO oxidation reaction, respectively [60].

Table 4
Average Pt particle size for the catalysts and their turnover frequencies (TOF) in the DHP reaction [22].

Catalyst	Particle size			TOF (s^{-1})[c]
	TEM	XRD[a]	H_2-chemisorption[b]	
Pt/SBA-15_WI	21	21	37	0.2
Pt/SBA-15_DP	3	~3	6.8	0.08

[a] Based on the Scherrer equation.
[b] Determined by d (nm) = 1.13/D (D = dispersion).
[c] TOF calculated, based on H_2-chemisorption data, from C_3H_8 conversion at 5 min.

They found that the Pt catalysts supported on SBA-15 showed much better activity and selectivity than that supported on γ-Al_2O_3, Fig. 25A, due to the mesopore characteristics of SBA-15, Table 5. The high surface area of SBA-15 ensures better dispersion of Pt NPs and smaller particle size, thus resulting in higher catalytic activity. The enhanced activity indicates that SBA-15 is better than γ-Al_2O_3 when used as support of Pt catalysts for VOCs oxidation.

Table 5
The physical properties of SBA-15 and γ-Al_2O_3 and that of the supported metal catalysts [134].

Catalysts	Surface area (m^2/g)	Pore volume (cm^3/g)	Avg. pore diameter (nm)	Metal dispersion [CO or (NO) chemisorption, %]
SBA-15	956	0.98	5.32	
γ-Al_2O_3	184	0.27	5.05	
Pt(1)[a]/SBA-15	920	0.95	5.23	35
Pt(1)/γ-Al_2O_3	169	0.25	4.99	18

[a] Metal loading (wt.%).

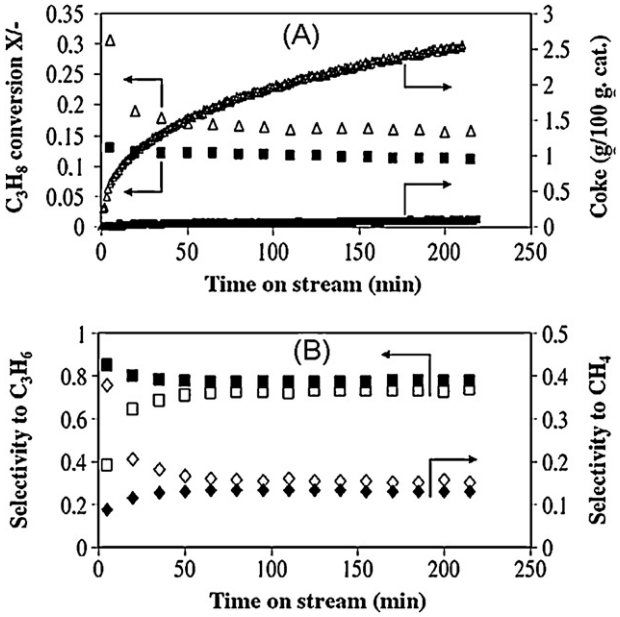

Fig. 24. Pt-SBA-15-WI (filled symbols) and Pt-SBA-15-DP (open symbols): (A) C_3H_8 conversion and coke formation during DHP and (B) selectivity to C_3H_6 (□, ■) and CH_4 (◇, ◆) [22].

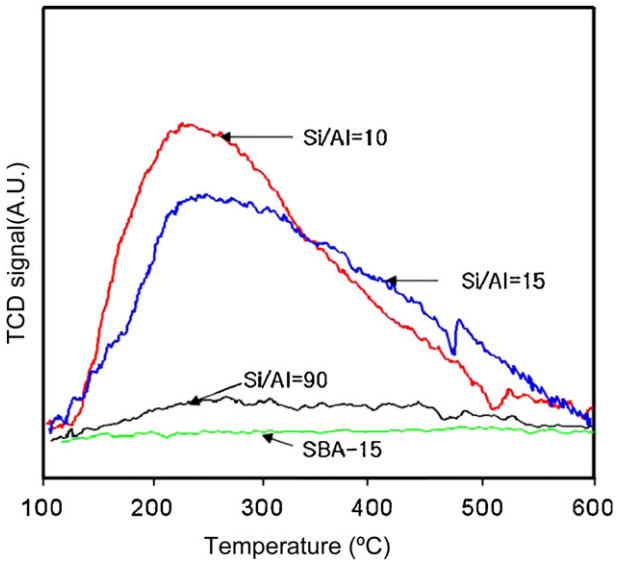

Fig. 26. NH_3-TPD spectra of SBA-15 and Al-SBA-15 supports [134].

The authors [134] also investigated the substitution of Al for Si on the activity of Pt/SBA-15, results of which indicated that the addition of Al facilitates the reaction to proceed, and the activity increases with the increase of Al content, Fig. 25B. This suggests that the catalytic performances of Pt/SBA-15 could be improved by incorporation of foreign cations into the SBA-15 framework. NH_3-TPD experiments [134] indicated that the incorporation of Al atoms enhanced the surface acidity of the SBA-15 framework, Fig. 26. Together with the catalytic activity and surface acidity, it is concluded that surface acidity of catalyst is a crucial parameter in deciding the catalytic activity of PAHs oxidation.

8.5. Aerobic selective oxidation of D-glucose to gluconic acid in liquid phase

Selective oxidation of alcohols by molecular oxygen in liquid phase is an attracting topic in organic chemistry, as it provides a green route for the synthesis of fine chemicals and intermediates. In contrast to the traditional routes, which use stoichiometric oxidants and release large amounts of pollutants [135,136], this is a sustainable route as the catalyst can be recycled and the only byproduct is water.

Table 6 lists the catalytic activities of D-glucose oxidation reactions carried out over Pt/SBA-15, with Pt loading of 1, 2, 3 wt.% (denoted as Pt_1/SBA-15, Pt_2/SBA-15, Pt_3/SBA-15, respectively), reported by Mai et al. [137]. Results indicated that the D-glucose was well converted and gluconic acid was the main product of each catalyst, with selectivity of ~86%. For catalyst with

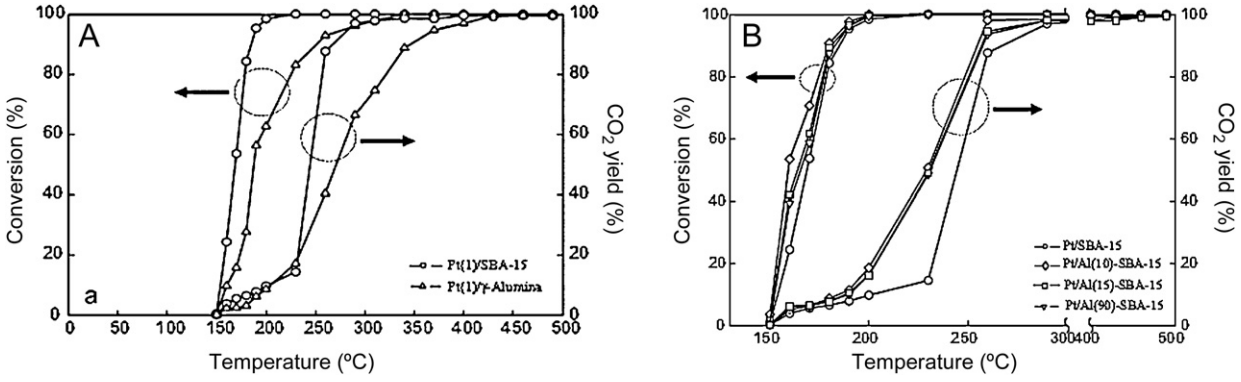

Fig. 25. Conversion of naphthalene and CO_2 yield over (A) Pt(1)/SBA-15 and Pt(1)/γ-Al_2O_3, (B) Pt/SBA-15 and Pt/Al-SBA-15 for catalytic oxidation of naphthalene [134].

Table 6
Results of the oxidation of D-glucose carried out over Pt/SBA-15 with different Pt loading (temperature: 80 °C; air flow rate: 20 mL/min; time: 2 h) [137].

Entry	Catalyst	Conversion (%)	Composition of products (%)			
			Gluconic acid	Lactone	Disaccharide	Other products
1	PS-1 (pH ~ 9)	74.54	86.63	3.16	8.20	2.01
2	PS-2 (pH ~ 9)	70.14	85.81	3.64	8.57	1.98
3	PS-3 (pH ~ 9)	48.87	86.56	3.25	8.11	2.08
4	PS-1 (pH*)	51.72	53.04	22.73	22.42	1.81

PS-*N* (*N* = 1, 2, 3): Pt/SBA-15 with Pt loading of 1, 2, 3 wt.%.
Other products: tartaric, threonic, acrylic acids, and the products of decarboxylation.
pH*: the oxidation reaction was performed without pH control.

different Pt loading, the conversion decreased with the increase of Pt loading, in sequence of Pt_1/SBA-15 > Pt_2/SBA-15 > Pt_3/SBA-15, indicating that higher Pt loading is not favorable for the reaction. In principle, higher Pt loading could lead to more active sites and higher activity if the Pt particle size is the same. The decreased activity observed here thus could be that the Pt particle size for catalyst with higher Pt loading is too big to be active for the reaction. Indeed, TEM measurements on the catalysts showed that the Pt average particle size of Pt_1/SBA-15 was below 6 nm, while that of Pt_2/SBA-15 and Pt_3/SBA-15 were in the range of 12–15 nm [137]. That is, large Pt particles that were inactive for the reaction were formed at high Pt loading, leading to fewer active Pt particles and lower activity. Also, as the Pt particle size in Pt_1/SBA-15 (<6 nm) is smaller than the pore diameter (6.77 nm) of SBA-15, the Pt particles can be attached inside the pores, forming additional active sites (besides those on the external surface) and thus enhancing the catalytic activity.

On the other hand, as is known that basicity is an important parameter of supported noble metal catalysts used for aerobic oxidation of alcohols in liquid phase, investigation on the effect of pH value on the reaction was also conducted by the authors. Catalytic performances of Pt_1/SBA-15 for D-glucose oxidation carried out with and without pH control were presented in the entries 1 and 4 of Table 6. Comparing with the reaction without pH control, both the conversion and the selectivity enhanced significantly when the pH was controlled at ~9 throughout the reaction, confirming that basicity is an important parameter for Pt/SBA-15 showing high activity for aerobic alcohol oxidation reaction, similar to that for supported Au catalysts [138,139].

9. Conclusions

In summary, Pt/SBA-15 has been proved to be one type of promising catalysts for heterogeneous catalysis due to its excellent performances exhibited in reactions such as CO oxidation, aerobic alcohol oxidation, and propane dehydrogenation. The SBA-15 support has high surface area, controllable pore size as well as high thermal stability, ensuring it to be a good support for the preparation of small, stable and active Pt NPs. Nevertheless, how to control the Pt particle size and stabilize the Pt NPs on the surface of SBA-15 is still a challenging topic of today, as the surface of SBA-15 is relatively inert and the Pt NPs tend to aggregate at high temperature and/or leaching in liquid phase. Future works thus should not only to explore new applications of Pt/SBA-15 in heterogeneous catalysis, but also to find new strategies to stabilize the Pt NPs during the reaction.

Acknowledgements

Financial supports from the National Science Foundation of China (Grant Nos. 21203254 and 21073238) and the Special Fund of the Central University Research, South-central University for Nationalities (CZZ11007) are gratefully acknowledged.

References

[1] A. Alavi, P. Hu, T. Deutsch, P.L. Silvestrelli, J. Hutter, Physical Review Letters 80 (1998) 3650.
[2] S.M. McClure, D.W. Goodman, Chemical Physics Letters 469 (2009) 1.
[3] Y.J. Mergler, A. van Aalst, J. van Delft, B.E. Nieuwenhuys, Applied Catalysis B: Environmental 10 (1996) 245.
[4] M. Niwa, K. Awano, Y. Murakami, Applied Catalysis 7 (1983) 317.
[5] R.P. Doherty, J.-M. Krafft, C. Méthivier, S. Casale, H. Remita, C. Louis, C. Thomas, Journal of Catalysis 287 (2012) 102.
[6] D.A. Hickman, L.D. Schmidt, AIChE Journal 39 (1993) 1164.
[7] J. Xu, X.-C. Xu, L. Ouyang, X.-J. Yang, W. Mao, J. Su, Y.-F. Han, Journal of Catalysis 287 (2012) 114.
[8] H. Igarashi, H. Uchida, M. Suzuki, Y. Sasaki, M. Watanabe, Applied Catalysis A: General 159 (1997) 159.
[9] A. Tsuji, K.T.V. Rao, S. Nishimura, A. Takagaki, K. Ebitani, ChemSusChem 4 (2011) 542.
[10] G. Avgouropoulos, T. Ioannides, C. Papadopoulou, J. Batista, S. Hocevar, H.K. Matralis, Catalysis Today 75 (2002) 157.
[11] T. Anastas Paul, C. Heine Lauren, W. Tracy, Green Chemical Syntheses and Processes, vol. 767, American Chemical Society, 2000, p. 1 (Chapter 1).
[12] M. Ilyas, M. Sadiq, Chemical Engineering and Technology 30 (2007) 1391.
[13] C. Xu, B.E. Koel, M.A. Newton, N.A. Frei, C.T. Campbell, Journal of Physical Chemistry 99 (1995) 16670.
[14] G. Aguilar-Ríos, P. Salas, M.A. Valenzuela, H. Armendáriz, J.A. Wang, J. Salmones, Catalysis Letters 60 (1999) 21.
[15] M. Aramendía, J. Benítez, V. Boráu, C. Jiménez, J. Marinas, A. Moreno, Reaction Kinetics and Catalysis Letters 62 (1997) 23.
[16] P. Sun, G. Siddiqi, W.C. Vining, M. Chi, A.T. Bell, Journal of Catalysis 282 (2011) 165.
[17] M.-L. Yang, Y.-A. Zhu, C. Fan, Z.-J. Sui, D. Chen, X.-G. Zhou, Physical Chemistry Chemical Physics 13 (2011) 3257.
[18] M. Anpo, N. Aikawa, Y. Kubokawa, Journal of Physical Chemistry 88 (1984) 3998.
[19] C. Lian, H. Liu, C. Xiao, W. Yang, K. Zhang, Y. Liu, Y. Wang, Chemical Communications 48 (2012) 3124.
[20] C.-S. Chen, H.-W. Chen, W.-H. Cheng, Applied Catalysis A: General 248 (2003) 117.
[21] M. Englisch, V.S. Ranade, J.A. Lercher, Applied Catalysis A: General 163 (1997) 111.
[22] S.M. Kumar, D. Chen, J.C. Walmsley, A. Holmen, Catalysis Communications 9 (2008) 747.
[23] A.P. Alivisatos, Science 271 (1996) 933.
[24] M.M. Schubert, S. Hackenberg, A.C. van Veen, M. Muhler, V. Plzak, R.J. Behm, Journal of Catalysis 197 (2001) 113.
[25] Z. Yan, S. Chinta, A.A. Mohamed, J.P. Fackler, D.W. Goodman, Journal of the American Ceramic Society 127 (2005) 1604.
[26] J. Yu, R. Wang, S. Ren, X. Sun, C. Chen, Q. Ge, W. Fang, J. Zhang, H. Xu, D.S. Su, ChemCatChem 4 (2012) 1376.
[27] A.S. Ivanova, E.M. Slavinskaya, R.V. Gulyaev, V.I. Zaikovskii, O.A. Stonkus, I.G. Danilova, L.M. Plyasova, I.A. Polukhina, A.I. Boronin, Applied Catalysis B: Environmental 97 (2010) 57.
[28] A. Manasilp, E. Gulari, Applied Catalysis B: Environmental 37 (2002) 17.
[29] S.S. Kim, H.H. Lee, S.C. Hong, Applied Catalysis B: Environmental 119–120 (2012) 100.
[30] W. Zhai, S. Xue, A. Zhu, Y. Luo, Y. Tian, ChemCatChem 3 (2011) 127.
[31] C.M. Kalamaras, P. Panagiotopoulou, D.I. Kondarides, A.M. Efstathiou, Journal of Catalysis 264 (2009) 117.
[32] A. Corma, A. Martıĭnez, V. Martıĭnez-Soria, Journal of Catalysis 169 (1997) 480.
[33] S.C. Shen, S. Kawi, Applied Catalysis B: Environmental 45 (2003) 63.
[34] R. Long, R. Yang, Catalysis Letters 52 (1998) 91.
[35] D.Y. Zhao, J.L. Feng, Q.S. Huo, N. Melosh, G.H. Fredrickson, B.F. Chmelka, G.D. Stucky, Science 279 (1998) 548.

[36] D.Y. Zhao, Q.S. Huo, J.L. Feng, B.F. Chmelka, G.D. Stucky, Journal of the American Ceramic Society 120 (1998) 6024.
[37] K. Cassiers, T. Linssen, M. Mathieu, M. Benjelloun, K. Schrijnemakers, P. Van Der Voort, P. Cool, E.F. Vansant, Chemistry of Materials 14 (2002) 2317.
[38] J.P. Thielemann, F. Girgsdies, R. Schlögl, C. Hess, Beilstein Journal of Nanotechnology 2 (2011) 110.
[39] P.I. Ravikovitch, A.V. Neimark, Journal of Physical Chemistry B 105 (2001) 6817.
[40] M. Kruk, M. Jaroniec, C.H. Ko, R. Ryoo, Chemistry of Materials 12 (2000) 1961.
[41] C.-M. Yang, B. Zibrowius, W. Schmidt, F. Schüth, Chemistry of Materials 16 (2004) 2918.
[42] X. Xu, H. Xu, F. Kapteijn, J.A. Moulijn, Applied Catalysis B: Environmental 53 (2004) 265.
[43] B. Lee, Z. Ma, Z. Zhang, C. Park, S. Dai, Microporous and Mesoporous Materials 122 (2009) 160.
[44] Z.J. Wang, Y.B. Xie, C.J. Liu, Journal of Physical Chemistry C 112 (2008) 19818.
[45] J.A. Singh, S.H. Overbury, N.J. Dudney, M. Li, G.M. Veith, ACS Catalysis 2 (2012) 1138.
[46] J. Yang, G. Mestl, D. Herein, R. Schlogl, J. Find, Carbon 38 (2000) 729.
[47] M. Ilyas, M. Saeed, International Journal of Chemical Reactor Engineering 8 (2010) A77.
[48] X.W. Xie, Y. Li, Z.Q. Liu, M. Haruta, W.J. Shen, Nature 458 (2009) 746.
[49] C.P. Rodrigues, V.T. da Silva, M. Schmal, Applied Catalysis B: Environmental 96 (2010) 1.
[50] T. Tsoncheva, L. Ivanova, J. Rosenholm, M. Linden, Applied Catalysis B: Environmental 89 (2009) 365.
[51] F. Wyrwalski, J.M. Giraudon, J.F. Lamonier, Catalysis Letters 137 (2010) 141.
[52] A. Szegedi, M. Popova, V. Mavrodinova, C. Minchev, Applied Catalysis A: General 338 (2008) 44.
[53] J.J. Zhu, K. Kailasam, A. Fischer, A. Thomas, ACS Catalysis 1 (2011) 342.
[54] H. Itoh, S. Utamapanya, J.V. Stark, K.J. Klabunde, J.R. Schlup, Chemistry of Materials 5 (1993) 71.
[55] X.W. Xie, W.J. Shen, Nanoscale 1 (2009) 50.
[56] A.Y. Khodakov, A. Griboval-Constant, R. Bechara, V.L. Zholobenko, Journal of Catalysis 206 (2002) 230.
[57] W.J. Shen, M. Okumura, Y. Matsumura, M. Haruta, Applied Catalysis A: General 213 (2001) 225.
[58] S. Rojluechai, S. Chavadej, J.W. Schwank, V. Meeyoo, Catalysis Communications 8 (2007) 57.
[59] H. Song, R.M. Rioux, J.D. Hoefelmeyer, R. Komor, K. Niesz, M. Grass, P.D. Yang, G.A. Somorjai, Journal of the American Ceramic Society 128 (2006) 3027.
[60] J. Zhu, X. Xie, S.A.C. Carabineiro, P.B. Tavares, J.L. Figueiredo, R. Schomacker, A. Thomas, Energy & Environmental Science 4 (2011) 2020.
[61] A.K. Prashar, R.P. Hodgkins, R. Kumar, R. Nandini Devi, Journal of Materials Chemistry 18 (2008) 1765.
[62] R. Ryoo, C.H. Ko, M. Kruk, V. Antochshuk, M. Jaroniec, Journal of Physical Chemistry B 104 (2000) 11465.
[63] A. Galarneau, H. Cambon, F. Di Renzo, F. Fajula, Langmuir 17 (2001) 8328.
[64] J. Zhu, K. Kailasam, X. Xie, R. Schomaecker, A. Thomas, Chemistry of Materials 23 (2011) 2062.
[65] E.B. Celer, M. Kruk, Y. Zuzek, M. Jaroniec, Journal of Materials Chemistry 16 (2006) 2824.
[66] M. Kruk, L. Cao, Langmuir 23 (2007) 7247.
[67] E.B. Celer, M. Jaroniec, Journal of the American Ceramic Society 128 (2006) 14408.
[68] S. Chytil, W.R. Glomm, I. Kvande, Z. Tiejun, E.A. Blekkan, Studies in Surface Science and Catalysis 162 (2006) 513.
[69] S. Chytil, W.R. Glomm, E.A. Blekkan, Catalysis Today 147 (2009) 217.
[70] J.H. Anderson jr, K.A. Wickersheim, Surface Science 2 (1964) 252.
[71] C.C. Perry, X. Li, Journal of the Chemical Society, Faraday Transactions 87 (1991) 3857.
[72] C.C. Perry, X. Li, Journal of the Chemical Society, Faraday Transactions 87 (1991) 761.
[73] C.C. Harrison, X. Li, I. Hopkinson, S.E. Stratford, A.G. Orpen, Journal of the Chemical Society, Faraday Transactions 89 (1993) 4115.
[74] T. Vrålstad, W.R. Glomm, M. Rønning, H. Dathe, A. Jentys, J.A. Lercher, G. Øye, M. Stöcker, J. Sjöblom, Journal of Physical Chemistry B 110 (2006) 5386.
[75] B.A. Morrow, A.J. McFarlan, Journal of Physical Chemistry 96 (1992) 1395.
[76] B. Humbert, Journal of Non-Crystalline Solids 191 (1995) 29.
[77] D.W. Sindorf, G.E. Maciel, Journal of the American Ceramic Society 105 (1983) 1487.
[78] J.S. Beck, J.C. Vartuli, W.J. Roth, M.E. Leonowicz, C.T. Kresge, K.D. Schmitt, C.T.W. Chu, D.H. Olson, E.W. Sheppard, Journal of the American Ceramic Society 114 (1992) 10834.
[79] G.E. Maciel, D.W. Sindorf, Journal of the American Ceramic Society 102 (1980) 7606.
[80] S. Chytil, W. Glomm, I. Kvande, T. Zhao, J. Walmsley, E. Blekkan, Topics in Catalysis 45 (2007) 93.
[81] Y.-J. Han, J.M. Kim, G.D. Stucky, Chemistry of Materials 12 (2000) 2068.
[82] J. Geus, A.J. Van Dillen, Preparation of Supported Catalysts by Deposition Precipitation, Wiley-VCH, Weinheim, 1999.
[83] J.T. Richardson, Book Principles of Catalyst Development, Plenum Press, New York, 1989.
[84] M.K. van der Lee, J. van Dillen, J.H. Bitter, K.P. de Jong, Journal of the American Ceramic Society 127 (2005) 13573.
[85] J.C.P. Broekhoff, J.H. de Boer, Journal of Catalysis 10 (1968) 377.
[86] A. Galarneau, M. Nader, F. Guenneau, F. Di Renzo, A. Gedeon, Journal of Physical Chemistry C 111 (2007) 8268.
[87] R.M. Rioux, H. Song, J.D. Hoefelmeyer, P. Yang, G.A. Somorjai, Journal of Physical Chemistry B 109 (2004) 2192.
[88] C.-m. Yang, P.-h. Liu, Y.-f. Ho, C.-y. Chiu, K.-j. Chao, Chemistry of Materials 15 (2002) 275.
[89] C.M. Yang, H.S. Sheu, K.J. Chao, Advanced Functional Materials 12 (2002) 143.
[90] L.X. Zhang, J.L. Shi, J. Yu, Z.L. Hua, X.G. Zhao, M.L. Ruan, Advanced Materials 14 (2002) 1510.
[91] W. Huang, J.N. Kuhn, C.-K. Tsung, Y. Zhang, S.E. Habas, P. Yang, G.A. Somorjai, Nano Letters 8 (2008) 2027.
[92] L. Sun, R.M. Crooks, Langmuir 18 (2002) 8231.
[93] R.W.J. Scott, O.M. Wilson, R.M. Crooks, Journal of Physical Chemistry B 109 (2004) 692.
[94] É. Molnár, Z. Kónya, G. Tasi, I. Kiricsi, in: N.Ž.J. Čejka, P. Nachtigall (Eds.), Stud. Surf. Sci. Catal., Part B, vol. 158, Elsevier, 2005, p. 1351.
[95] T. Wang, H. Shou, Y. Kou, H. Liu, Green Chemistry 11 (2009) 562.
[96] T.S. Ahmadi, Z.L. Wang, T.C. Green, A. Henglein, M.A. El-Sayed, Science 272 (1996) 1924.
[97] Y.M.A. Yamada, T. Arakawa, H. Hocke, Y. Uozumi, Angewandte Chemie International Edition 46 (2007) 704.
[98] T. Wang, C.-X. Xiao, L. Yan, L. Xu, J. Luo, H. Shou, Y. Kou, H. Liu, Chemical Communications (2007) 4375.
[99] L. Qiu, F. Liu, L. Zhao, W. Yang, J. Yao, Langmuir 22 (2006) 4480.
[100] T. Herricks, J. Chen, Y. Xia, Nano Letters 4 (2004) 2367.
[101] P.R. Van Rheenen, M.J. McKelvy, W.S. Glaunsinger, Journal of Solid State Chemistry 67 (1987) 151.
[102] M.R. Knecht, M.G. Weir, V.S. Myers, W.D. Pyrz, H. Ye, V. Petkov, D.J. Buttrey, A.I. Frenkel, R.M. Crooks, Chemistry of Materials 20 (2008) 5218.
[103] Y. Borodko, C.M. Thompson, W. Huang, H.B. Yildiz, H. Frei, G.A. Somorjai, Journal of Physical Chemistry C 115 (2011) 4757.
[104] M.J. Hossain, H. Tsunoyama, M. Yamauchi, N. Ichikuni, T. Tsukuda, Catalysis Today 183 (2012) 101.
[105] H. Ye, R.W.J. Scott, R.M. Crooks, Langmuir 20 (2004) 2915.
[106] R.M. Crooks, M. Zhao, Advanced Materials 11 (1999) 217.
[107] O. Ozturk, T.J. Black, K. Perrine, K. Pizzolato, C.T. Williams, F.W. Parsons, J.S. Ratliff, J. Gao, C.J. Murphy, H. Xie, H.J. Ploehn, D.A. Chen, Langmuir 21 (2005) 3998.
[108] O.S. Alexeev, A. Siani, G. Lafaye, C.T. Williams, H.J. Ploehn, M.D. Amiridis, Journal of Physical Chemistry B 110 (2006) 24903.
[109] D. Liu, J. Gao, C.J. Murphy, C.T. Williams, Journal of Physical Chemistry B 108 (2004) 12911.
[110] R.W.J. Scott, C. Sivadinarayana, O.M. Wilson, Z. Yan, D.W. Goodman, R.M. Crooks, Journal of the American Ceramic Society 127 (2005) 1380.
[111] R.W.J. Scott, O.M. Wilson, R.M. Crooks, Chemistry of Materials 16 (2004) 5682.
[112] S. Chytil, W.R. Glomm, E. Vollebekk, H. Bergem, J. Walmsley, J. Sjöblom, E.A. Blekkan, Microporous and Mesoporous Materials 86 (2005) 198.
[113] Z. Kónya, V.F. Puntes, I. Kiricsi, J. Zhu, A.P. Alivisatos, G.A. Somorjai, Nano Letters 2 (2002) 907.
[114] J. Zhu, Z. Kónya, V.F. Puntes, I. Kiricsi, C.X. Miao, J.W. Ager, A.P. Alivisatos, G.A. Somorjai, Langmuir 19 (2003) 4396.
[115] A.K. Prashar, R.P. Hodgkins, J.N. Chandran, P.R. Rajamohanan, R.N. Devi, Chemistry of Materials 22 (2010) 1633.
[116] H. Song, R.M. Rioux, J.D. Hoefelmeyer, R. Komor, K. Niesz, M. Grass, P. Yang, G.A. Somorjai, Journal of the American Ceramic Society 128 (2006) 3027.
[117] S.H. Joo, J.Y. Park, C.-K. Tsung, Y. Yamada, P. Yang, G.A. Somorjai, Nature Materials 8 (2009) 126.
[118] N.W. Cant, R.A. Donaldson, Journal of Catalysis 78 (1982) 461.
[119] H. Bischoff, N.I. Jaeger, G.Z. Schulz-Ekloff, Zeitschrift fur Physikalische Chemie (Leipzig) 271 (1990) S1093.
[120] G. Djéga-Mariadassou, M. Boudart, Journal of Catalysis 216 (2003) 89.
[121] A.D. Allian, K. Takanabe, K.L. Fujdala, X. Hao, T.J. Truex, J. Cai, C. Buda, M. Neurock, E. Iglesia, Journal of the American Ceramic Society 133 (2011) 4498.
[122] M. Boudart, A.W. Aldag, L.D. Ptak, J.E. Benson, Journal of Catalysis 11 (1968) 35.
[123] S.D. Lin, M.A. Vannice, Journal of Catalysis 143 (1993) 554.
[124] S.D. Lin, M.A. Vannice, Journal of Catalysis 143 (1993) 563.
[125] J. Chupin, N.S. Gnep, S. Lacombe, M. Guisnet, Applied Catalysis A: General 206 (2001) 43.
[126] L. Bednarova, C.E. Lyman, E. Rytter, A. Holmen, Journal of Catalysis 211 (2002) 335.
[127] O.A. Bariås, A. Holmen, E.A. Blekkan, Journal of Catalysis 158 (1996) 1.
[128] T. Waku, J.A. Biscardi, E. Iglesia, Journal of Catalysis 222 (2004) 481.
[129] R.T. Vang, K. Honkala, S. Dahl, E.K. Vestergaard, J. Schnadt, E. Laegsgaard, B.S. Clausen, J.K. Norskov, F. Besenbacher, Nature Materials 4 (2005) 160.
[130] Y. Zhang, Y. Zhou, K. Yang, Y. Li, Y. Wang, Y. Xu, P. Wu, Microporous and Mesoporous Materials 96 (2006) 245.
[131] F. Wyrwalsky, J.-F. Lamonier, S. Siffert, A. Aboukais, Applied Catalysis B 70 (2007) 393.
[132] E.C. Moretti, N. Mukhopadhyay, Chemical Engineering Progress 89 (1993) 20.
[133] International Program on Chemical Safety (IPCS), Environmental Health Criteria 2002, Selected Non-heterocyclic Polycyclic Aromatic Hydrocarbons, WHO, Geneva, 1998.

[134] J. Park, J.-K. Lee, J. Miyawaki, S.-H. Yoon, I. Mochida, Journal of Industrial and Engineering Chemistry 17 (2011) 271.
[135] D.G. Lee, U.A. Spitzer, Journal of Organic Chemistry 35 (1970) 3589.
[136] K.P.C. Vollhardt, N.E. Schore, Organic Chemistry: Structure and Function, Freeman, New York, 1999, p. 300.
[137] T.T.N. Mai, N.T.M. Thu, P.D. Trong, N.T. Ha, G.T.P. Ly, VNU Journal of Science, Nature Science and Technology 26 (2010) 183.
[138] J.J. Zhu, J.L. Figueiredo, J.L. Faria, Catalysis Communications 9 (2008) 2395.
[139] T. Mallat, A. Baiker, Chemical Reviews 104 (2004) 3037.